university of groningen / faculty of science and engineering / mathematics and applied mathematics

Surface knots, ch-diagrams, and the knot group

Bachelor's Project Mathematics

Student: Jamara Admiraal, S4989686, j.m.admiraal@student.rug.nl

First supervisor: prof. dr. R.I. van der Veen

Second supervisor: dr. N. Martynchuk

Contents

Abstract

This thesis investigates surface knots, that is, closed connected surfaces in four-space. We begin by introducing the core notions for working with surface knots and reviewing several standard representations, with a particular focus on ch-diagrams and *ab*-surfaces. These serve as a tool for visualizing and manipulating surface knots to help determine when two surface knots are equivalent. Building upon the well-established theory for classical knots, we discuss the Wirtinger presentation to determine the knot group, which is an important algebraic invariant given by the fundamental group of the knot complement. Using ch-diagrams, we derive an altered version of the Wirtinger presentation that describes the knot group of surface knots. Furthermore, we explore the construction of (twist-)spun knots, which are obtained by spinning classical knots in four-space, and compute their associated knot groups using the developed presentation method. The results obtained from the adapted Wirtinger presentation are cross-referenced with known results in the literature to verify their consistency and correctness.

Acknowledgments

Before getting into the main contents of this text, I would like to extend my sincerest thanks to a number of people who have played a vital role in producing this thesis in one way or another.

My first supervisor, prof. dr. R.I. van der Veen, for providing excellent advice, guidance, and mathematical inspiration throughout the writing of this thesis. I also want to thank him for his exceptional execution and teaching of the course *Algebraic Topology*, which played a significant part in solidifying which areas of mathematics interest me most, and a number of the concepts introduced there play a crucial role in this text.

My second supervisor, dr. N. Martynchuk, for aiding in the assessment of this thesis.

My wonderful friends for their mental support, technical aid, and never-ending belief in my abilities. In particular, Jard and Milène.

Lastly, my dear partner Tijmen for their irreplaceable support and encouragement. It is always a joy to share mathematics and everything else in life with you.

1 Introduction

Knot theory is a well-known and widely studied field within mathematics. Typically, this study concerns itself with knottings of the circle $\mathbb{S}^1$, i.e. a knot is a set $k \subset \mathbb{R}^3$ which is homeomorphic to $\mathbb{S}^1$. We refer to this study of knottings of $\mathbb{S}^1$ as *classical* knot theory. In general, we denote by $\mathbb{S}^n$ the standard n-sphere, by $\mathbb{R}^n$ real n-dimensional space, and by $\mathbb{B}^n$ the standard n-dimensional ball.

There are a multitude of tools available to study classical knots. For example, knots are typically represented by a *knot diagram*, and two knots can be shown to be equivalent through *Reidemeister moves* on such a diagram. Additionally, many so-called *knot invariants* exist, which provide a way of distinguishing different knots based on some of their properties; if two knot diagrams differ with respect to some knot invariant, they must represent different knots. A particularly well-known example of a knot invariant is the *knot group*, i.e. the fundamental group of the knot complement.

A natural question is whether this notion of classical knots can be generalized to higher dimensions, i.e. whether we can define n-knots $K \subset \mathbb{R}^{n+2}$ homeomorphic to $\mathbb{S}^n$ for $n > 1$. While this is indeed possible, an immediate difficulty presents itself: classical knot theory is often very visual. How do we visualize sets of dimension 4 or higher? If we do manage to define an analogy to knot diagrams, can we find a set of moves similar to Reidemeister moves for equivalent n-knots? Do invariants for n-knots exist, for example a knot group (i.e. the fundamental group of $\mathbb{R}^{n+2} \setminus K$)? Throughout this thesis, we aim to explore these questions for 2-*knots* homeomorphic to $\mathbb{S}^2$ embedded in 4-space. We also consider other kinds of *surface knots*, which are submanifolds in 4-space homeomorphic to a closed connected surface other than $\mathbb{S}^2$.

Around 1900, important contributions to classical knot theory were made by researchers like Reidemeister and Wirtinger, who worked together to develop this field. Notably, Wirtinger showed how to determine the knot group of a given classical knot. Extending the study of classical knot theory to surface knots was first done by Artin in 1925 in [Art25] by defining spun knots, a way of creating higher-dimensional surfaces from classical knots. This construction was later generalized to twist-spinning by Zeeman in [Zee65]. Around the same time, mathematicians like Fox worked on developing diagrammatic tools for studying surface knots, most notably the motion pictures as introduced in [Fox62]. In the past three decades, these diagrammatic methods were further development by Yoshikawa, Carter, Saito, and Kamada (among others). Some particularly noteworthy contributions around this time include [Yos94], [SS98], and [Kam17].

Chapter 2 covers some preliminaries required for understanding the main body of this thesis. This includes some topics in classical knot theory, as well as a brief introduction to group presentations, homotopy, and the fundamental group.

Chapter 3 provides a general introduction to surface knots. We discuss when two surfaces are considered equivalent, and introduce a number of tools that

make it easier to see this equivalence in practice, most notably ch-diagrams and Yoshikawa moves. Motion pictures and *ab*-surfaces are introduced to aid in the visualization of surface knots. Additionally, we discuss an explicit way to construct a 2-knot from a given classical knot through the process of (twist-)spinning. Figure 1.1 shows the spun trefoil and its motion picture.

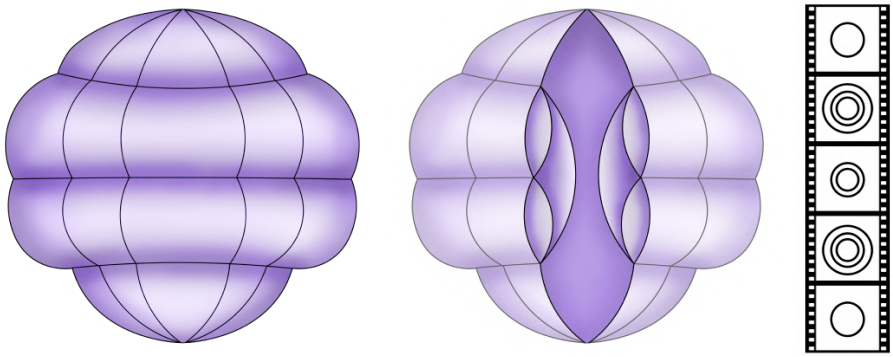

Figure 1.1: The spun knot obtained from the trefoil knot, this same knot with a wedge removed, and the corresponding motion picture.

Finally, Chapter 4 aims to generalize a well-known tool from classical knot theory to surface knots. The Wirtinger presentation is usually applied to knot diagrams of classical knots, but it turns out this method may easily be adapted to ch-diagrams, producing the knot group of a surface knot. We also briefly touch upon the knot group of (twist-)spun knots, as their knot group is closely related to the knot group of the corresponding classical knot.

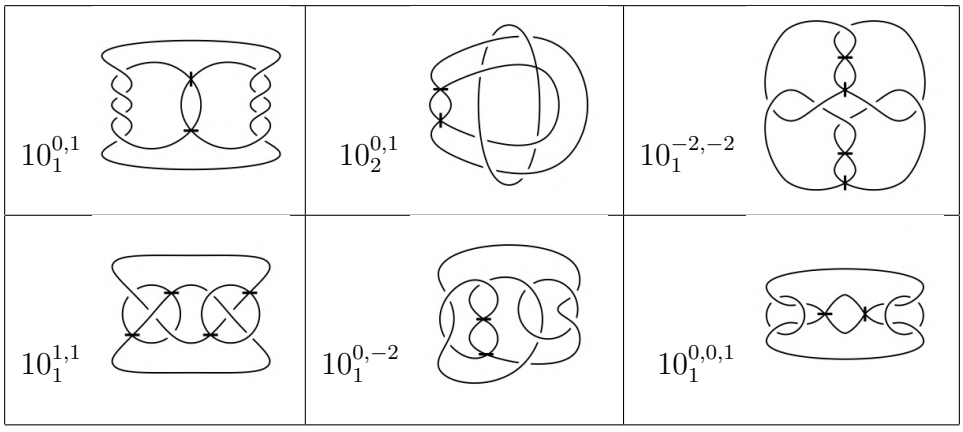

Table 1: A number of ch-diagrams.

Appendix A. provides a table of ch-diagrams of all weakly prime surfaces up to ch-index 10, as adapted from [Yos94, ch. 5]. It also lists their knot groups based

on these ch-diagrams as determined through the adapted Wirtinger presentation. Table 1 provides a preview of some of the ch-diagrams presented in this appendix.

As is common within knot theory, we only consider (classical and surface) knots which are piecewise linear, as this prevents pathological complications [Rol03, ch. 1.A]. For more details on piecewise linear topology, see [RS82]. Additionally, we require our surface knots to be locally flat, adapting the definition as in [Rol03, ch. 2.G]. This means each point on a surface knot K has a closed neighbourhood N in $\mathbb{R}^4$ such that $(N, N \cap K)$ is homeomorphic as a pair to the standard ball pair $(\mathbb{B}^4, \mathbb{B}^2)$. Being homeomorphic as a pair entails that there is a homeomorphism f between N and $\mathbb{B}^4$ such that the restriction $f\big|_{N\cap K}$ is a homeomorphism between $N \cap K$ and $\mathbb{B}^2$.

We remark that the illustrations presented throughout this text were created specifically for this thesis by the author. As such, no references for the figures are provided.

2 Preliminaries

2.1 Classical knot theory

This section provides a brief introduction to classical knot theory based on [Kam17, ch. 2.1], to which we refer for additional references. We treat only those core concepts required for understanding Chapters 3 and 4. For a more general introduction to classical knot theory, we refer to a book like [Ada04] or [Rol03].

Definition 2.1. A *classical knot* k is a submanifold[1] of $\mathbb{R}^3$ which is PL-homeomorphic to $\mathbb{S}^1$.

Definition 2.2. A *classical link* k with c components is a union of c mutually disjoint classical knots k_i, such that

$$k = \bigcup_{i=1}^{c} k_i.$$

The classical knots k_i are called the *components* of k.

For a classical knot (or link) k, let $\iota : k \to \mathbb{R}^3$ denote the inclusion map, and let $p_0 : \mathbb{R}^3 \to \mathbb{R}^2$ be the projection onto the (x, y)-plane. Consider their composition $f : k \to \mathbb{R}^2$, $f = p_0 \circ \iota$.

Definition 2.3. We say that k is in *general position* with respect to the projection p_0 when f is an immersion[2] and all its multiple points[3] are double points such that the tangent directions of the two elements of $f^{-1}(p)$ cross transversely. The image $f(k)$ is called a *regular projection*, see Figure 2.1a.

In this way, the only self-intersections of $f(k)$ are *crossings*, preventing strands from touching (rather than crossing), or having more than two strands cross in one multiple point.

Definition 2.4. A crossing p has inverse image consisting of two distinct points, say q and q', such that the z-coordinate of q is greater than that of q'. The point q is called the *overcrossing point*, and q' is called the *undercrossing point*. For a small neighbourhood $N(p)$ of p, the inverse image $f^{-1}(N(p))$ consists of two arcs, say a and a' such that $q \in a$ and $q' \in a'$. The arc a is called the *overcrossing* (or *over arc*), and a' is the *undercrossing* (or *under arc*).

Definition 2.5. A *knot diagram* of a knot is its regular projection equipped with the over- and undercrossing information at each crossing.

[1] Informally, a submanifold is a subset that locally looks like Euclidean space of lower dimension. For a formal definition, see [Lee13].

[2] The composition f is called an immersion if the differential $D_p f$ is injective for all values $p \in k$. In this scenario, this simplifies to the derivative of f vanishing nowhere.

[3] A point $p \in f(k)$ is called a multiple point if $f^{-1}(p)$ consists of strictly more than one point.

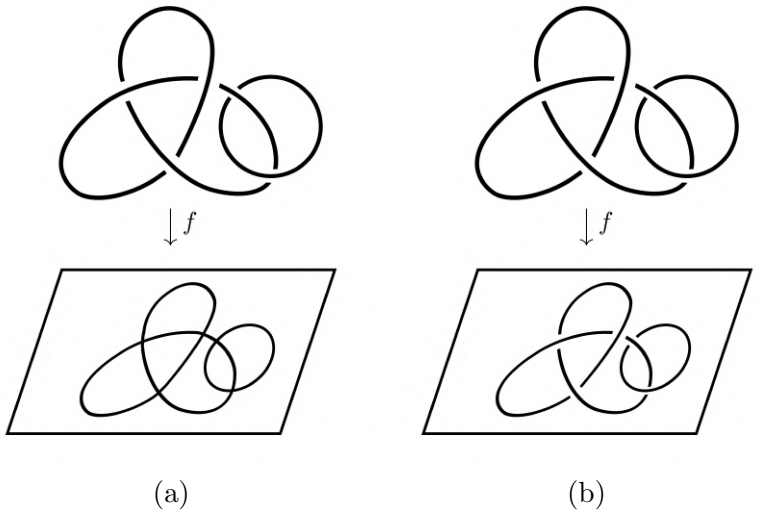

(a) (b)

Figure 2.1: A regular projection (left) and a knot diagram (right).

Typically, displaying the over- and undercrossing information in a knot diagram is done by removing a small under arc from $f(k)$ as seen in Figure 2.1b.

An *orientation* of a knot k is an orientation of k as a 1-manifold, which is denoted in its knot diagram by placing coherently directed arrows along the diagram in the direction of choice. An orientation of a link is given by assigning an orientation to each of its components. The *mirror image* of a knot is obtained by changing every overcrossing to an undercrossing as illustrated in Figure 2.2.

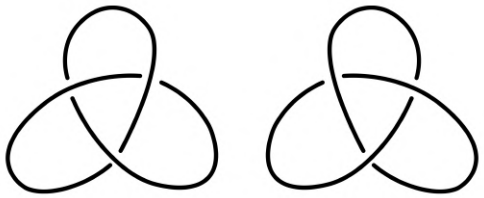

Figure 2.2: The trefoil knot and its mirror image.

One of the main questions within the field of knot theory is when two knots are considered equivalent.

Definition 2.6. Two subsets A_1, A_2 of a space X are called *ambient isotopic in* X if there exists a homeomorphism $H : X \times [0,1] \to X \times [0,1]$ such that

1. For all $s \in [0,1]$, there exists a homeomorphism $h_s : X \to X$ satisfying $H(x,s) = (h_s(x), s)$ for all $x \in X$;
2. $h_0 = \mathrm{id}$;
3. $h_1(A_1) = A_2$.

Two classical knots (or links) are said to be equivalent if they are ambient isotopic in $\mathbb{R}^3$. Informally, an ambient isotopy between two knots describes how one can be continuously deformed into the other by distorting the ambient space, without letting the knot break or self-intersect. Figure 2.3 shows a number of non-equivalent knots, and a link.

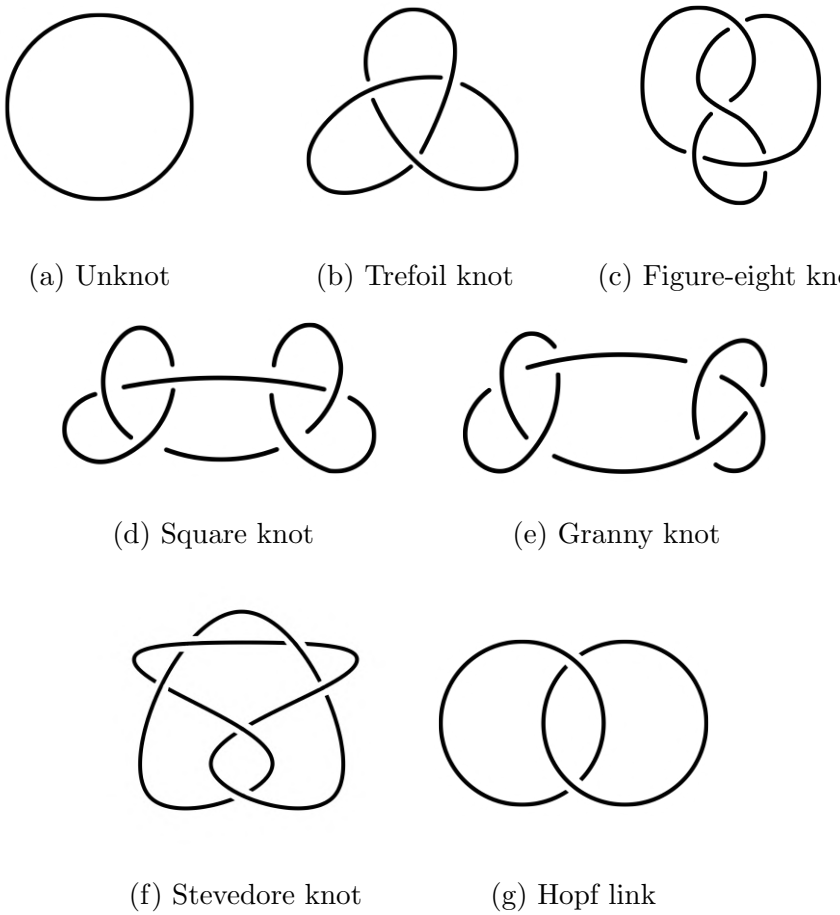

(a) Unknot (b) Trefoil knot (c) Figure-eight knot

(d) Square knot (e) Granny knot

(f) Stevedore knot (g) Hopf link

Figure 2.3: Knot diagrams of several non-equivalent knots and a link.

Definition 2.7. A classical knot is *trivial* or *unknotted* if it is equivalent to $\mathbb{S}^1$, and a classical link is trivial if each of its components is trivial.

Famously, there exists a set of moves on knot diagrams to describe when the corresponding knots are equivalent. In practice, these moves are often much easier to work with than constructing explicit ambient isotopies of $\mathbb{R}^3$.

Definition 2.8. The local operations defined on knot diagrams as in Figure 2.4 are called *Reidemeister moves* of type I, II, and III respectively.

Theorem 2.9 (Reidemeister's theorem)**.** *Two classical knots (or links) are equivalent if and only if their knot diagrams are related by a finite sequence of Reidemeister moves and ambient isotopies of* $\mathbb{R}^2$*.*

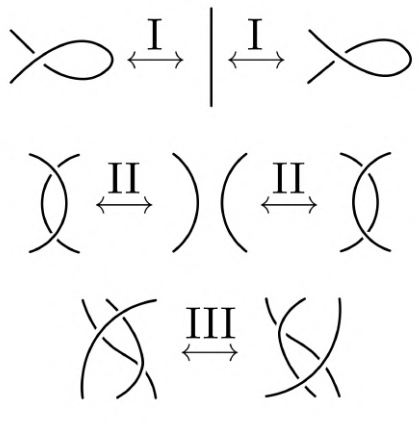

Figure 2.4: Reidemeister moves of types I, II, and III.

Remark. Reidemeister moves and Reidemeister's theorem generalize to oriented knot diagrams in the natural way.

A swift way of creating new knots from any two given knots is through their composition, which also provides a tool in defining which classical knots function as "core building blocks". The following definitions are adapted from [Ada04, ch. 1.2].

Definition 2.10. Given two knot diagrams which do not overlap, their *composition* is given by removing a small arc not containing any crossings from either diagram, and then connecting the four resulting endpoints so that the two diagrams are now connected without introducing any new crossings as illustrated in Figure 2.5. The composition of two classical knots k_1, k_2 is denoted by $k_1 \# k_2$.

Remark. Composition of knots is a well-defined operation.

Definition 2.11. A classical knot is called a *composite knot* if it can be expressed as the composition of two classical knots, neither of which is the unknot. If it cannot be expressed as such, it is called a *prime knot*.

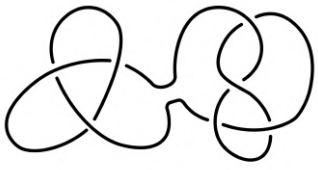

Figure 2.5: The composition of two knots.

We conclude this section with a brief introduction to braids, following the definitions in [Ada04, ch. 5.4]. A *braid* is a collection of n strings which are attached

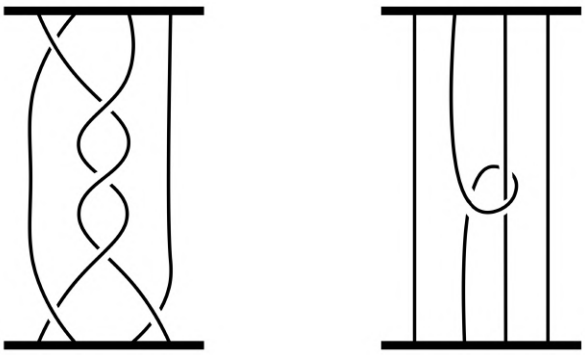

(a) A braid. (b) Not a braid.

Figure 2.6

to a bar at the top and bottom, in which each string intersects any horizontal plane between the bars only once, i.e. each strand only moves downwards when following it from the top bar to the bottom bar. Figure 2.6 illustrates when a collection of strands form a braid. For a formal defintion of a braid, we refer to [Kam02, ch. 1].

To acquire a classical knot or link from a braid, one must apply a *closure* to the braid, which is a set way of connecting the loose ends of the strands. Most commonly, this is done by glueing the top and bottom bars together as illustrated in Figure 2.7a. For the purpose of this text we consider a different type of closure, namely the so-called *plat closure* of a braid with an even number of strands. In a plat closure, each pair of consecutive endpoints at the top is connected with a simple arc, and so is each pair of consecutive endpoints at the bottom [nLa25] as illustrated in Figure 2.7b.

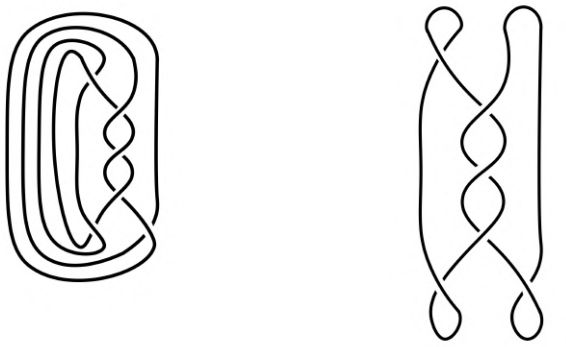

(a) The usual closure. (b) Plat closure.

Figure 2.7: Two different closures of the braid presented in Figure 2.6a.

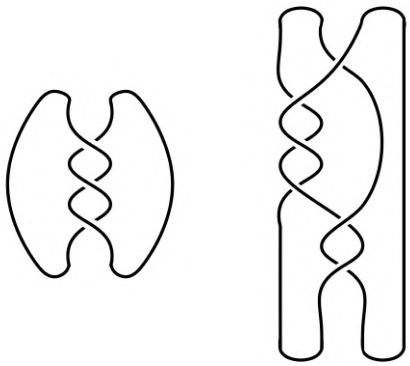

Figure 2.8: The four-plat of the trefoil (left) and figure-eight (right) knots.

We have the following result for classical knots with bridge number[4] up to 2 as presented in [All+23, ch. 4].

Lemma 2.12. *Every 2-bridge knot can be represented as taking the plat closure of a braid on four strands, of which the rightmost strand does not contain any crossings.*

Definition 2.13. A classical knot in the form of Lemma 2.12 is called a *four-plat (knot)*.

While it might seem particularly restrictive to list this result which applies only to those classical knots with bridge number up to 2, it is important to note that this includes all non-trivial prime classical knots with up to 7 crossings [Ada04, ch. 3.2]. This means it includes common examples used throughout this thesis, including the trefoil and figure-eight knots. Figure 2.8 shows the four-plat of the trefoil and figure-eight, and Figure 2.9 shows how to derive that of the figure-eight.

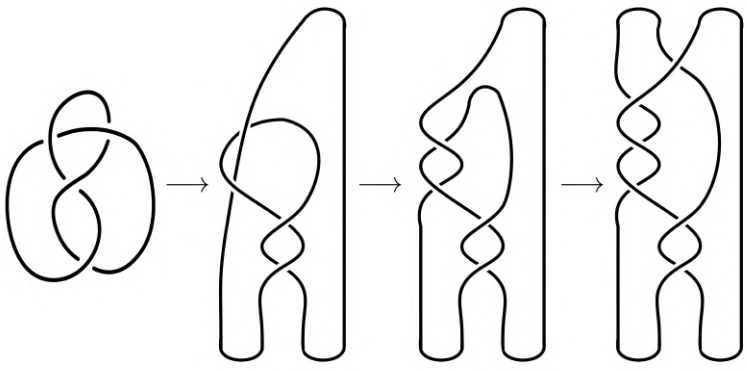

Figure 2.9: Constructing the four-plat of the figure-eight knot.

[4]For details on the bridge number of a classical knot, we refer to [Ada04, ch. 3.2].

2.2 Group presentations

One method of forming a group is using a so-called presentation of said group, which provides a concrete tool in the computation of the fundamental group of many spaces, including the complement of (classical and surface) knots. This section provides a brief introduction, but one may refer to most undergraduate texts regarding abstract algebra for more details on group presentations, like [DF03].

Definition 2.14. A *word* is any written product of group elements (and their inverses). The *free group* F_S on a set S consists of all words that can be built from the elements of S.

Example 2.15. If $S = \{x, y, z\}$, then some examples of words in the elements of S are

$$xy^{-1}xz^{-1}y, \;\; xyz, \;\; xxxyyzy^{-1}y^{-1}x^{-1}x^{-1}x^{-1},$$

where the latter is commonly written as

$$x^3y^2zy^{-2}x^{-3},$$

which is not a word itself but rather shorthand notation for one. △

Example 2.16. If S is a singleton set, then $F_S \cong \mathbb{Z}$. △

Definition 2.17. Let S be a set, and R be a set of words on S. Take N to be the smallest normal subgroup containing R. Then, the quotient

$$F_S/N,$$

is a *group presentation* of a group G if it is isomorphic to G, denoted by $\langle S \mid R \rangle$. The sets S and R are the *generators* and *relators* of the presentation.

Remark. Every group is isomorphic to many different group presentations, and it may be very difficult to determine whether two presentations are isomorphic.

Intuitively, we want G to be as free as possible on the given generators, subject only to the relations given by R (such that for each $r \in R$, $r = 1$). In some cases, a relator might be given by a relation if it provides additional clarification. For example, we may write $ab = ba$ instead of $aba^{-1}b^{-1}$. Throughout this text, we concern ourselves mainly with *finite presentations*, meaning both the set of generators and the set of relators are finite. Let us consider a few examples of familiar groups.

Example 2.18. The cyclic group of order n has group presentation $\langle a \mid a^n \rangle$. △

Example 2.19. If $R = \varnothing$, then $\langle S \mid R \rangle$ presents the free group on S. △

Example 2.20. The free Abelian group of rank 2 is presented by $\langle a, b \mid ab = ba \rangle$, which is isomorphic to $\mathbb{Z}^2$. △

Example 2.21. The dihedral group D_n of order $2n$ has group presentation

$$\langle \rho, \mu \mid \rho^n, \mu^2, (\rho\mu)^2 \rangle,$$

where ρ denotes a rotation and μ denotes a reflection. △

2.3 Homotopy and the fundamental group

To define the fundamental group of a topological space, we must introduce the notion of homotopy.

Definition 2.22. For topological spaces X, Y and continuous maps $f, g : X \to Y$, we say f is *homotopic* to g if there exists a continuous map $H : X \times [0,1] \to Y$ such that for all $x \in X$,

1. $H(x,0) = f(x)$;
2. $H(x,1) = g(x)$.

For a subset A of X, if $H(a,t) = f(a) = g(a)$ for all $a \in A$ and $t \in [0,1]$, then f is *homotopic to g relative to A*, denoted by $f \overset{H}{\simeq}_A g$. If it is evident which homotopy is being referred to, or if $A = \varnothing$, one may omit the H or A respectively.

Intuitively, two maps are homotopic if their graphs can be continuously deformed into each other. A homotopy relative to a subset keeps the elements of the subset fixed. Figure 2.10 provides an illustration. We note that homotopy defines an equivalence relation, as is shown in [Hat01, ch. 1.1]. This equivalence relation is still well-defined when taking homotopy relative to a set A.

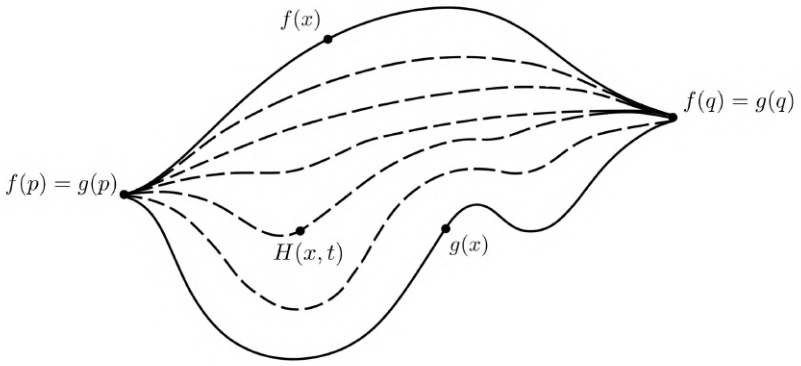

Figure 2.10: Illustrating homotopy between maps f, g relative to $\{p, q\}$.

Definition 2.23. Two spaces X and Y are *homotopy equivalent* if there exist continuous maps $f : X \to Y$ and $g : Y \to X$ satisfying

$$f \circ g \simeq \mathrm{id}_Y,$$
$$g \circ f \simeq \mathrm{id}_X .$$

Homotopy equivalence is denoted by $X \simeq Y$.

To define the fundamental group, we are in particular interested in homotopies between loops centered at the same base point p, i.e. homo-

topies $H : [0,1] \times [0,1] \to Y$ between continuous maps $f, g : [0,1] \to Y$ relative to $\{0,1\}$ such that $f(0) = f(1) = p$. Taking the equivalence classes of such homotopic maps relative to $\{0,1\}$ forms a group under concatenation as shown in [Hat01, ch. 1.1].

Definition 2.24. The group of homotopy classes of loops in X based at p under concatenation is called the *fundamental group*, denoted by $\pi_1(X, p)$.

We note that in path-connected spaces the dependence on a base point is redundant, in which case we may simply write $\pi_1(X)$. Additionally, we have the following as seen in [Hat01, ch. 1.1].

Theorem 2.25. *If $f : X \to Y$ is a homotopy equivalence, then the fundamental groups of these spaces are isomorphic as groups, i.e.*

$$\pi_1(X, p) \cong \pi_1(Y, f(p)).$$

In more complicated spaces, directly computing the fundamental group is often highly non-trivial. However, these spaces may be split up into smaller spaces which are easier to work with, in which case the following theorem allows us to compute the fundamental group of the original space through these smaller spaces.

Theorem 2.26 (Seifert-van Kampen)**.** *Let U and V be open, path-connected spaces such that their intersection is non-empty and path-connected, and $\pi_1(U \cap V)$ is finitely generated. If*

$$\langle g_1, \ldots, g_{n_1} \mid q_1, \ldots, q_{m_1} \rangle, \quad \langle h_1, \ldots, h_{n_2} \mid r_1, \ldots, r_{m_2} \rangle,$$

are group presentations for $\pi_1(U)$ and $\pi_1(V)$ respectively, then the fundamental group of $U \cup V$ can be presented by

$$\langle g_1, \ldots, g_{n_1}, h_1, \ldots, h_{n_2} \mid q_1, \ldots, q_{m_1}, r_1, \ldots, r_{m_2}, u_1 v_1^{-1}, \ldots, u_k v_k^{-1} \rangle,$$

where u_i and v_i, $i = 1, \ldots k$ denote the generators of $\pi_1(U \cap V)$ in terms of $\pi_1(U)$ and $\pi_1(V)$ respectively.

This version of the Seifert-van Kampen Theorem is adapted from [BW03, ch. 6]. For a more general version not reliant on group presentations, one may refer to a text on (algebraic) topology, like [Hat01, ch. 1.2] or [Mun14, ch. 9].

Let us consider an example.

Example 2.27. Consider the space presented in Figure 2.11, the union of two circles A and B whose intersection is a single point p.

The fundamental group of each circle A and B becomes clear when seeing them as a loop with a single "hole". Looping around one of these hole once gives us a generator (say g_1 for A, and g_2 for B), and we may loop around any number of times. Two paths can only be homotopy equivalent if they loop around the

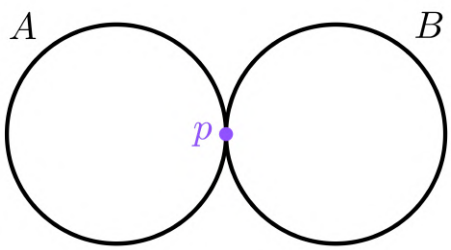

Figure 2.11: The union of two circles whose intersection is a point p.

same number of times, and there are no additional constraints, meaning we have no generators. Thus,

$$\pi_1(A) \cong \langle g_1 \mid \varnothing \rangle \cong \mathbb{Z} \cong \langle g_2 \mid \varnothing \rangle \cong \pi_1(B).$$

For a more formal argument, refer to [Hat01, ch. 1.1].

Now, consider the union of the two circles. Let U be A and a small open section of B, such that $U \simeq A$. Similarly, take V as B and a small open section of A, such that $V \simeq B$. Then, $U \cap V$ is an open path-connected neighbourhood of p with $U \cap V \simeq p$. We thus have that

$$\pi_1(U \cap V) \cong \pi_1(p) \cong \{1\},$$

meaning there are no generators of $\pi_1(U \cap V)$ in terms of $\pi_1(U)$ or $\pi_1(V)$. We conclude by Theorem 2.26 that

$$\pi_1(A \cup B) \cong \langle g_1, g_2 \mid \varnothing \rangle,$$

the free group on two elements. △

3 Surface knots

In this chapter, we provide a general introduction to the concept of surface knots. To aid in this, we introduce two common visualization methods, namely motion pictures and ch-diagrams. We discuss when surface knots are considered to be equivalent by means of Yoshikawa moves. Additionally, an explicit construction for producing surface knots based on a classical knot is discussed, the so-called (twist-)spun knots. Throughout the chapter, a number of visual examples are provided to better illustrate the introduced concepts.

Throughout this text, the terms knot and surface knot may be used interchangeably. When referring to knottings of $\mathbb{S}^1$ as discussed in Section 2.1, we explicitly state they are classical knots.

Definition 3.1. A *surface knot* K is a submanifold of $\mathbb{R}^4$ which is PL-homeomorphic to a closed connected surface. If K is PL-homeomorphic to $\mathbb{S}^2$, it is called a 2-*knot*.

The main focus of this text lies on 2-knots, but for some (visual) examples we consider other categories of knots. For example, so-called T^2-knots, P^2-knots, and Kb-knots are homeomorphic to a torus, a projective plane, and a Klein bottle respectively. We refer the reader to [Kam17] for more details on these different categories of surface knots.

Definition 3.2. A *surface link* K with c components is a union of c mutually disjoint surface knots K_i, such that

$$K = \bigcup_{i=1}^{c} K_i.$$

The surface knots K_i are called the *components* of K and need not all be of the same category of surface knot.

Remark. Often, we do not explicitly distinguish between surface knots and links. The terms may be used interchangeably, or we simply speak of a surface.

Definition 3.3. Take a surface link K. If there exists a hyperplane separating K into two disjoint surface links (or knots) K_1, K_2, then K is called the *split union* of K_1 and K_2.

3.1 Equivalence of surface knots

Analogously to classical knots, we say two surface knots K_1 and K_2 are equivalent if they are ambient isotopic in $\mathbb{R}^4$, which we denote by $K_1 \cong K_2$ [Kam17, ch. 1.1-2]. While this way of defining equivalence of knots is clear and concise, it does not provide much practical insight for when two knots are in fact equivalent, since constructing an explicit ambient isotopy is often non-trivial. As such, the rest of this section introduces a number of tools that build up to Theorem 3.14, which provides a practical and convenient way to show two knots are equivalent.

Definition 3.4. We say a 2-knot K is *knotted* (or *non-trivial*) if there does not exist an ambient isotopy such that $K \cong \mathbb{S}^2$.

One tool commonly used to analyze surface knots is a so-called motion picture. Intuitively, a motion picture of a surface knot is a collection of x-ray images or cross sections of said knot. This allows us to visualize the structure of knotted surfaces through a series of projections. To this end, we regard $\mathbb{R}^4$ as the product $\mathbb{R}^3 \times \mathbb{R}$, where $\mathbb{R}^3$ is 3-dimensional Euclidean space, and $\mathbb{R}$ functions as a time parameter. Consider the projections

$$\begin{aligned} p_1 : \mathbb{R}^4 = \mathbb{R}^3 \times \mathbb{R} \to \mathbb{R}^3, \qquad & (x, y, z, t) \mapsto (x, y, z), \\ p_2 : \mathbb{R}^4 = \mathbb{R}^3 \times \mathbb{R} \to \mathbb{R}, \qquad & (x, y, z, t) \mapsto t. \end{aligned}$$

Definition 3.5. A *motion picture* (also called *movie*) of a surface knot K is the one-parameter family $\{p_1(K \cap p_2^{-1}(t))\}_{t \in \mathbb{R}}$.

Figure 3.1 shows two examples of a motion picture. Typically, a movie only displays those values of t for which each projection is a classical knot (or link), presented by a knot diagram [SS98, ch. 1.4] given that we include the over- and undercrossing information. As such, we emphasize that motion pictures live in $\mathbb{R}^3$, even if they are typically represented as two-dimensional images.

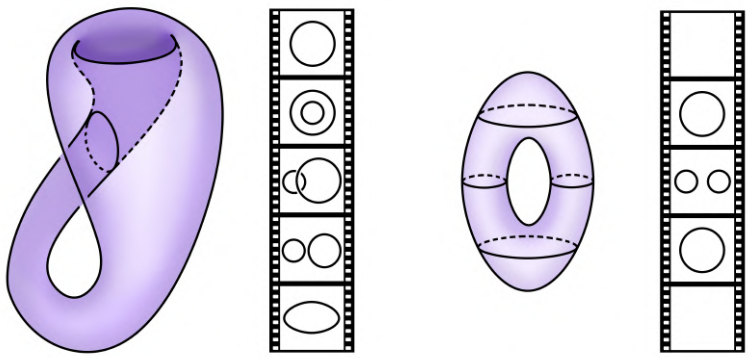

(a) (b)

Figure 3.1: A motion picture of a Klein bottle (left) and a torus (right).

Definition 3.6. If the cross section $p_1(K \cap p_2^{-1}(t_0))$ at $t = t_0$ is a classical link in $\mathbb{R}^3 \times \{t_0\}$, or the empty set, then t_0 is called a *regular value*. Otherwise, it is called a *critical value*.

By applying an appropriate ambient isotopy, we may assume that all critical values in $\mathbb{R}$ appear discretely [Ino13, ch. 2.2], [Kam17, ch. 3.1]. Another way of viewing this is that all critical points of K lie in distinct hyperplanes, and that there are finitely many of them. In fact, after such an appropriate ambient

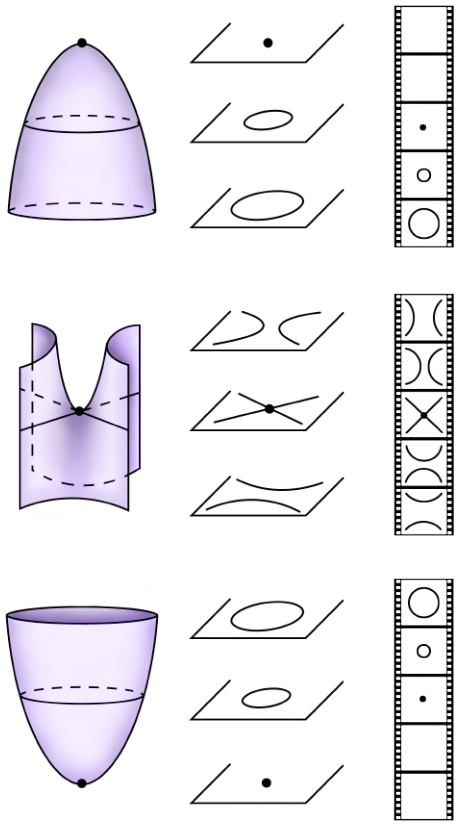

Figure 3.2: Elementary critical points.

isotopy, critical points take on one of three forms: they appear as either *maximal points*, *saddle points*, or *minimal points* [Kam02, ch. 8.2] as illustrated in Figure 3.2. These non-degenerate critical points are called *elementary critical points.*

Knowing that each surface knot is equivalent to a surface knot which only has elementary critical points, it follows that successive diagrams within a motion picture will differ by at most five types of critical changes as described in [SS98, ch. 1.4]. For an illustration, see Figure 3.3.

Theorem 3.7. *The critical changes we might encounter in successive frames of a motion picture are exclusively of the following types:*

1. *The birth (or death) of a simple closed curve;*
2. *A saddle point;*
3. *A type I Reidemeister move, the addition (or reduction) of a crossing;*
4. *A type II Reidemeister move, the addition (or reduction) of two crossings;*
5. *A type III Reidemeister move.*

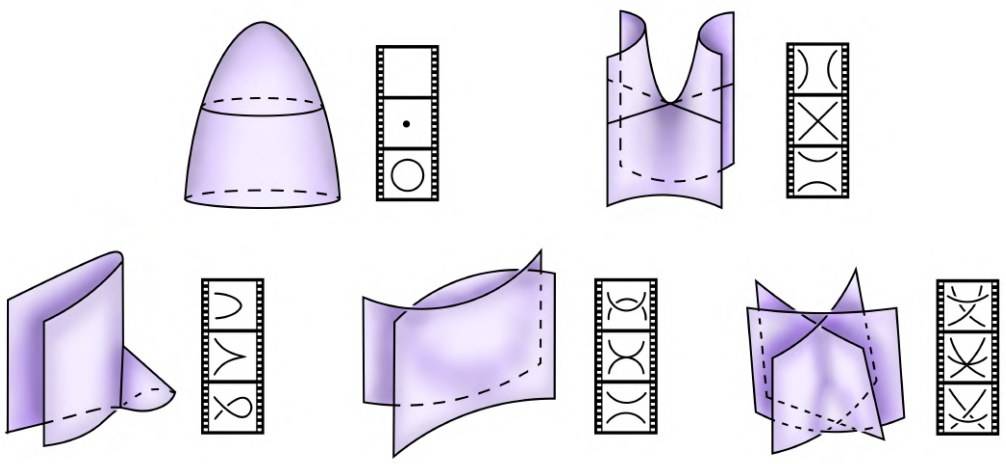

Figure 3.3: The five types of critical changes, where the middle frame of the motion picture is taken at the critical value.

Additionally, as every surface knot is equivalent to a knot with only elementary critical points, we may use the location of these elementary critical points to standardize the way knots are represented in a motion picture as described in the following theorem from [SS98, ch. 1.9][5].

Theorem 3.8. *Any surface knot is ambient isotopic to a surface knot satisfying the following conditions:*

1. *All its critical points are elementary critical points;*
2. *All its maximal points appear at the level $t = 1$;*
3. *All its saddle points appear at the level $t = 0$;*
4. *All its minimal points appear at the level $t = -1$.*

Definition 3.9. A surface knot satisfying the conditions of Theorem 3.8 is called a *hyperbolic splitting*.

The explicit form of a hyperbolic splitting is described in [Kam17, Thm. 3.2.1].

The rearrangements of critical points described here can be interpreted as Morse moves on the height function used to define the hyperbolic splitting of the surface in $\mathbb{R}^4$ into simpler pieces. In this sense, the procedure fits into the framework of Morse theory, which studies how the topology of a manifold changes as one passes through critical levels of a smooth function. For details on Morse theory, we refer to [Mil63].

[5]The existence of this form is a consequence of so-called *normal forms*, which are described in [Kam17, p. 3.2]. The existence of normal forms for orientable surface knots is shown [KSS82, ch. 2], while that for non-orientable surface knots is proven in [Kam89].

3.2 Ch-diagrams

The hyperbolic splitting of a surface knot allows us to fully reconstruct the original surface from the cross section at $t = 0$ to which we add a set of marks indicating in which direction the points above a saddle point (i.e. for $t > 0$) open up. This leads us to define the following representation for surface knots as introduced in [Yos94, ch. 2]. Definitions are additionally adapted from [Kam17, ch. 3.6] and [SS98, ch. 1.9].

Definition 3.10. A *ch-diagram* of a surface knot K is the cross-section $p_1(K \cap p_2^{-1}(0))$ at $t = 0$ of a hyperbolic splitting of K, in which marks indicate the directions of the saddle points. For small $0 < \varepsilon < 1$, the link $L_+ := K \cap (\mathbb{R}^3 \times \{\varepsilon\})$ is acquired by splitting the crossings along the marks, and $L_- := K \cap (\mathbb{R}^3 \times \{-\varepsilon\})$ is acquired by splitting the crossings in the direction perpendicular to the marks as illustrated in Figure 3.4.

Remark. In some cases we speak of a *ch-link*. This term indicates a slice of the hyperbolic splitting with the saddle markers added rather than its projection onto the cross section at $t = 0$, i.e. the set $p_1(K \cap p_2^{-1}([-\varepsilon, \varepsilon]))$.

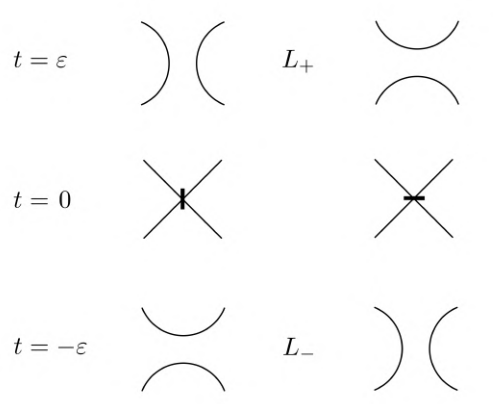

Figure 3.4: The links L_+ and L_- acquired by splitting crossings of a ch-diagram along the mark for positive time, and in the perpendicular direction for negative time.

The name ch-diagram comes from the elements such a diagram is made up of: the c stands for crossings, and the h for hyperbolic points (i.e. the marked saddle points). The set of all ch-diagrams presenting a given surface knot is denoted $\mathcal{D}$, and the set of all its ch-links is denoted $\mathcal{L}$. Figure 3.5 illustrates a ch-diagram of the spun trefoil knot, and a motion picture of its hyperbolic splitting based on this ch-diagram.

The following definition allows us to combine two given surfaces, and analyze their ch-diagram accordingly.

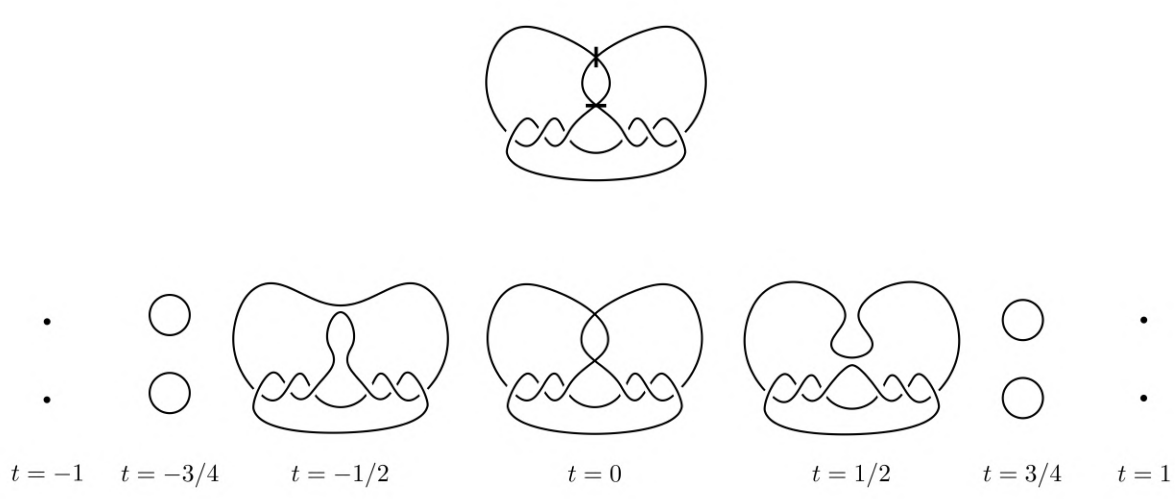

Figure 3.5: A ch-diagram and a motion picture of the hyperbolic splitting of the spun trefoil, adapted from [Yos94, ch. 2].

Definition 3.11. Consider the split union of K_1, K_2 with points $p_1 \in K_1$ and $p_2 \in K_2$. Consider small 4-balls $\mathbb{B}^4_1$ and $\mathbb{B}^4_2$ centered around p_1 and p_2 respectively such that $\mathbb{B}^4_1 \cap \mathbb{B}^4_2 = \varnothing$. In this way, $K_1 \cap \mathbb{B}^4_1$ and $K_2 \cap \mathbb{B}^4_1$ are a 2-disk. Remove the interior of these 2-disks from K_1 and K_2 respectively, creating a boundary on each of these surfaces equivalent to $\mathbb{S}^1$. We then connect these two boundary circles with a copy of $\mathbb{S}^1 \times [0,1]$, identifying $\mathbb{S}^1 \times \{0\}$ with the boundary circle on K_1 and $\mathbb{S}^1 \times \{1\}$ with the boundary circle on K_2. The resulting surface K is the *connected sum* of K_1 and K_2, denoted by $K = K_1 \# K_2$.

Remark. The connected sum of surfaces in 4-space is a well-defined operation [Kam17, ch. 1.2], [Yos94, ch. 2]. Additionally, ch-diagrams behave nicely under connected sums of surfaces, and their resulting composition is defined analogously to that of knot diagrams as in Definition 2.10.

While there are many different types of diagrams that may describe equivalent knots, ch-diagrams are connected by a collection of relatively simple moves.

Definition 3.12. The local operations in Figure 3.6 are called *Yoshikawa moves* named $\Omega_1, \ldots, \Omega_8$. It is understood that this includes the mirror images of the illustrated moves by changing the over/under information at each crossing, like in move Ω'_4 in Figure 3.6a.

We distinguish Yoshikawa moves of type I and type II. Those of type I act on ch-diagrams and correspond to ambient isotopies of $\mathbb{R}^3$, while moves of type II are defined on ch-links and describe ambient isotopies of $\mathbb{R}^4$ [Cht24, ch. 3], [Kam17, ch. 3.6].

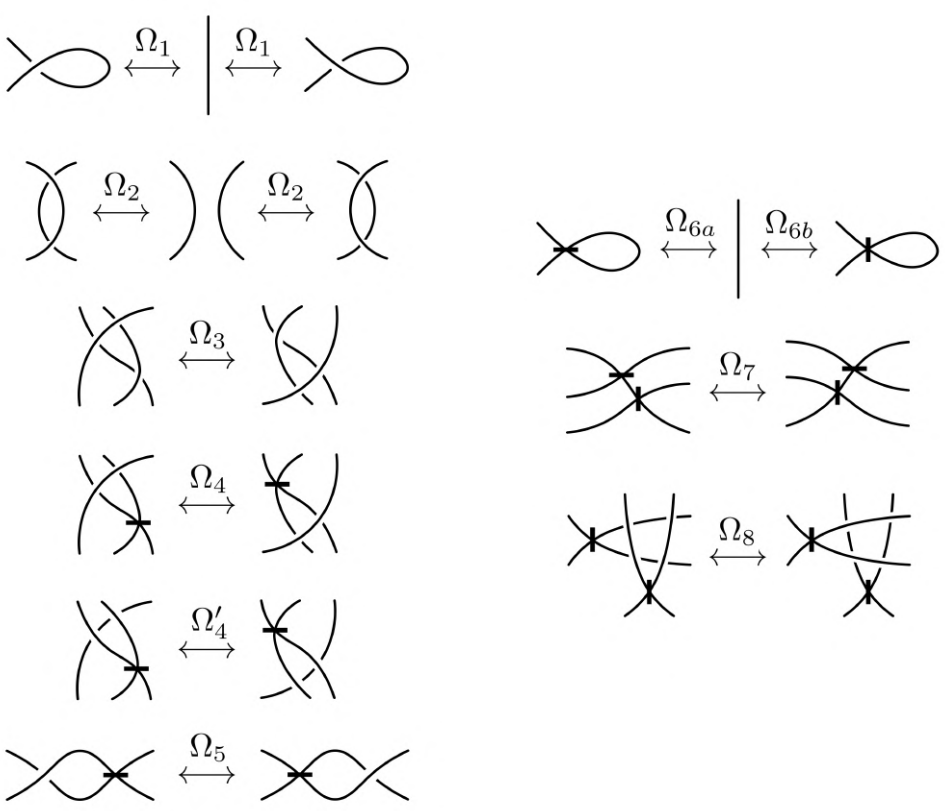

(a) Type I moves (b) Type II moves

Figure 3.6: Yoshikawa moves on ch-diagrams.

Definition 3.13. Two ch-diagrams are said to be *ch-equivalent*[6] if they are related by a finite sequence of Yoshikawa moves $\Omega_1, \ldots, \Omega_8$ and ambient isotopies of $\mathbb{R}^2$. Two ch-links are ch-equivalent when their ch-diagrams are.

It is well-known that Yoshikawa moves on ch-diagrams can be realized through ambient isotopies of $\mathbb{R}^4$ [KSS82], and thus that two ch-equivalent ch-diagrams represent equivalent surface knots. In fact, it turns out ch-diagrams and Yoshikawa moves also provide us with the exact tools to show two knots are equivalent, as first conjectured by Yoshikawa in [Yos94, ch. 2] and later proven in [Swe01].

Theorem 3.14. *Two ch-diagrams represent two equivalent surface knots if and only if they are ch-equivalent.*

Let us consider a few examples to gain some intuition for working with Yoshikawa moves.

[6]Yoshikawa uses the term *stably equivalent*.

Example 3.15. We show the move Ω_5 also holds with a vertical marker, as illustrated in Figure 3.7.

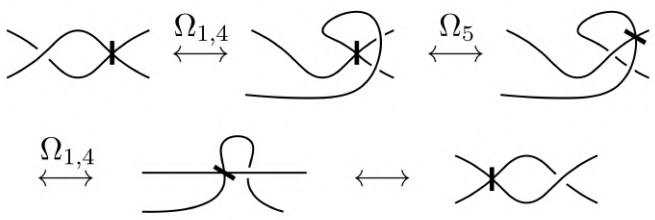

Figure 3.7: The Yoshikawa move Ω_5 also holds with a vertical marker, which follows from moves $\Omega_{1,4,5}$

△

Example 3.16. When two identical markers are directly connected by an arc, then we may reduce this to just one such marker as seen in Figure 3.8.

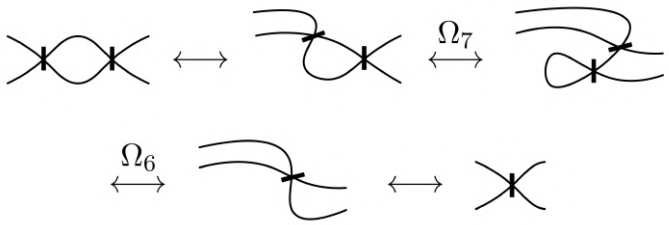

Figure 3.8: Reducing the number of saddles in a ch-diagram through Yoshikawa moves $\Omega_{6,7}$ when two identical markers are directly connected by an arc.

△

Ch-diagrams additionally provide a tool for classifying surface knots. For a ch-diagram $D \in \mathcal{D}$, let $c(D)$ denote the number of crossings of D, and $h(D)$ the number of hyperbolic points. Then,

$$ch(D) \coloneqq c(D) + h(D).$$

Example 3.17. If $D \in \mathcal{D}$ satisfies $ch(D) = 0$, then it consists of a number of circles in the plane and represents a trivial 2-knot [Kam17, ch. 3.6]. △

Interestingly, a ch-diagram of a surface K allows us to easily read off the Euler characteristic $\chi(K)$. It has been established in Morse theory that

$$\chi(K) = \#(\text{minima}) + \#(\text{maxima}) - \#(\text{saddle points}),$$

as seen in [Mil63, ch. 5]. This formula translates to ch-diagrams immediately; each component of the trivial link L_- corresponds to a minimum, each component

of the trivial link L_+ corresponds to a maximum, and the number of saddles is given by $h(D)$.

Theorem 3.18. *The Euler characteristic $\chi(K)$ of a surface K is given by*

$$\chi(K) = \#(\textit{components of } L_-) + \#(\textit{components of } L_+) - h(D).$$

Example 3.19. If $h(D) = 0$, i.e. the ch-diagram is a classical link diagram, then L_+ and L_- are the same and both consists of n components. Subsequently,

$$\chi(K) = n + n - 0 = 2n.$$

It follows that the corresponding surface is a surface link of n components, which are all trivial 2-knots. There may be possible visual "intersections" which give the crossings, but as $h(D) = 0$, there are no actual topological intersections. △

Definition 3.20. The *ch-index* of a surface knot K is given by

$$\mathrm{ch}(K) \coloneqq \min_{D \in \mathcal{D}} ch(D).$$

Remark. The ch-index is an invariant in the sense that two equivalent surface knots will have the same ch-index. However, like most invariants, it is not complete as many inequivalent surface knots share their ch-index. For example, the torus and projective plane both have ch-index equal to 2.

Lemma 3.21. *There does not exist a surface knot or link K with* $\mathrm{ch}(K) = 1$.

Proof. Suppose such a knot K exists, meaning it has a ch-diagram $D \in \mathcal{D}$ such that $ch(D) = 1$. This means D has either one crossing, or one marked saddle point. These can be resolved by Ω_1 or $\Omega_{6a,b}$ respectively, resulting in a ch-diagram $D' \in \mathcal{D}$ presenting K with $ch(D') = 0$. This is a contradiction, as the ch-index is the minimum value of ch over all diagrams in $\mathcal{D}$ and may thus not be smaller than $\mathrm{ch}(K) = 1$. □

As seen in [Yos94, ch. 2], when a link K is the split union of K_1 and K_2, we have that

$$\mathrm{ch}(K) = \mathrm{ch}(K_1) + \mathrm{ch}(K_2).$$

This becomes clear by considering two minimal ch-diagrams D_1 and D_2 for K_1 and K_2 respectively. As K is a split union, D_1 and D_2 may be placed far apart in the plane as two disjoint components. This disjoint union $D_1 \cup D_2$ then cannot be reduced further using Yoshikawa moves, and is thus a minimal ch-diagram for K. As we are simply counting the number of crossings in two disjoint diagrams, we see that $ch(D_1 \cup D_2) = ch(D_1) + ch(D_2)$. The result follows.

When a surface link K is a connected sum of two surface links K_1, K_2, a less strong result holds as presented in [Yos94, ch. 2], namely

$$\mathrm{ch}(K) \leq \mathrm{ch}(K_1) + \mathrm{ch}(K_2).$$

Yoshikawa questions whether this equation becomes an equality in case that both K_1 and K_2 are orientable. When at least one of K_1, K_2 is non-orientable, we know of examples for which the inequality is strict.

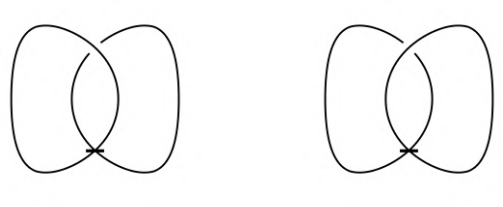

(a) P_+ (b) P_-

Figure 3.9: Ch-diagrams of the standard projective planes, from [Yos94, ch. 2].

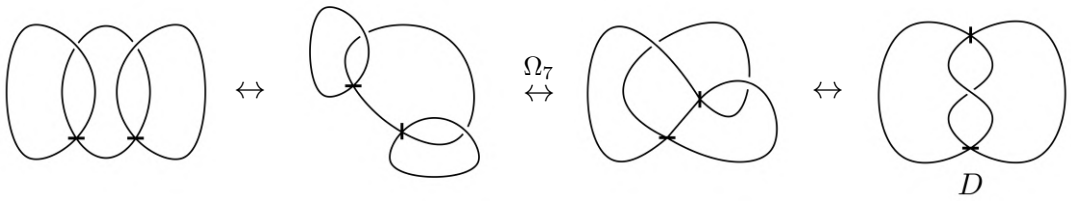

Figure 3.10: Showing a ch-diagram of the connected sum of the two standard projective planes is ch-equivalent to the ch-diagram D satisfying $ch(D) = 3$.

Example 3.22. Consider a ch-diagram of the standard projective planes P_+ and P_- as in Figure 3.9, each with ch-index equal to 2. Consider Figure 3.10, such that $ch(D) = 3$ and thus

$$\mathrm{ch}(P_+ \# P_-) \leq ch(D) = 3 < 4 = \mathrm{ch}(P_+) + \mathrm{ch}(P_-).$$

△

Example 3.23. Let K be any non-trivial 2-knot such that $\mathrm{ch}(K) > 0$. Then, the connected sum of K and P_+ is equivalent to P_+, and thus

$$\mathrm{ch}(K \# P_+) = \mathrm{ch}(P_+) = 2 < \mathrm{ch}(K) + \mathrm{ch}(P_+).$$

△

Definition 3.24. A surface link K is called *weakly prime* if it is not a connected sum of any two surface links K_1, K_2 satisfying $\mathrm{ch}(K_i) < \mathrm{ch}(K),\ i = 1, 2$.

In fact, it is reasonable to list all weakly prime surfaces, as justified by the theorem below.

Theorem 3.25. *Every surface K in $\mathbb{R}^4$ satisfies one of the following.*

1. *K is weakly prime;*
2. *K is a connected sum of finitely many weakly prime surface links, say $K_1, \ldots, K_n$, satisfying $\mathrm{ch}(K_i) < \mathrm{ch}(K),\ i = 1, \ldots, n,\ n \geq 2$.*

Proof. The statement follows by induction on $\mathrm{ch}(K)$. If $\mathrm{ch}(K) = 0$, K is a trivial 2-knot and thus weakly prime. Suppose $\mathrm{ch}(K) > 0$. If K is weakly prime, we are done. If K is not weakly prime, there exists surface links K_1, K_2 such that $K = K_1 \# K_2$ and $\mathrm{ch}(K_i) < \mathrm{ch}(K),\ i = 1, 2$.

If K_1, K_2 are both weakly prime, the statement holds. Suppose one of them, say K_i, is not weakly prime. As $\mathrm{ch}(K_i) < \mathrm{ch}(K)$, it follows by the induction hypothesis that K_i is a connected sum of finitely many weakly prime surface links $K_{i_1}, \ldots, K_{i_{n_i}}$ satisfying $\mathrm{ch}(K_{i_j}) < \mathrm{ch}(K),\ j = 1, \ldots, n_i$. Thus, K is a connected sum of finitely many weakly prime surface links. □

Table 2 is adapted from [Yos94, ch. 5] and lists all weakly prime surfaces in $\mathbb{R}^4$ up to ch-index 10. All the surface links listed are distinct from one another. We denote by $I_\ell^{g_1,\ldots g_c}$ a surface with ch-index equal to I consisting of c components with corresponding genera g_i. The subscript ℓ denotes the ℓ-th surface knot with ch-index equal to I with genera $g_1, \ldots, g_c$. For a 2-knot (consisting of one component with genus zero), we write $I_\ell^0 = I_\ell$. We use negative genera to indicate non-orientable components.

Example 3.26. 2_1^{-1} presents the projective plane, whereas 2_1^1 presents a standard torus. △

Example 3.27. The surface link $10_1^{0,-2}$ has ch-index equal to 10 and consists of two components, one a 2-knot and one a Kb-knot. △

A number of the surfaces in Table 2 are familiar in nature (e.g. (twist-)spun knots as introduced in Chapter 3.4), as described in Table 3.

3.3 *ab*-surfaces

While ch-diagrams allow us to fully reconstruct the original surface knot represented by a movie, it is not always evident what the hyperbolic splitting looks like as a surface as one may notice from Figures 3.5 and 3.11. As such, let us introduce another tool for analyzing surface knots based on their ch-diagrams, as described in [Cht24, ch. 3], from which the definitions provided here are adapted.

Definition 3.28. An *ab-surface* is a compact surface with boundary in $\mathbb{R}^3$ for which we assign a label from the set $\{a, b\}$ to each of its boundary components. Each component of the *ab*-surface has at least one boundary component corresponding to each label from $\{a, b\}$, and the a- and b-labelled boundary links are trivial.

Two *ab*-surfaces are considered equivalent if they are diffeomorphic[7] and have matching labelling on their boundaries. The set of all *ab*-surfaces is denoted by $\mathcal{AB}$. We define three *ab*-moves on these surfaces as given in Figure 3.12. The boundary links corresponding to the a- and b- labels are often colored in purple and green respectively to help distinguish them.

[7] A diffeomorphism is a smooth bijective map between manifolds that has a smooth inverse; see [Lee13] for a formal definition.

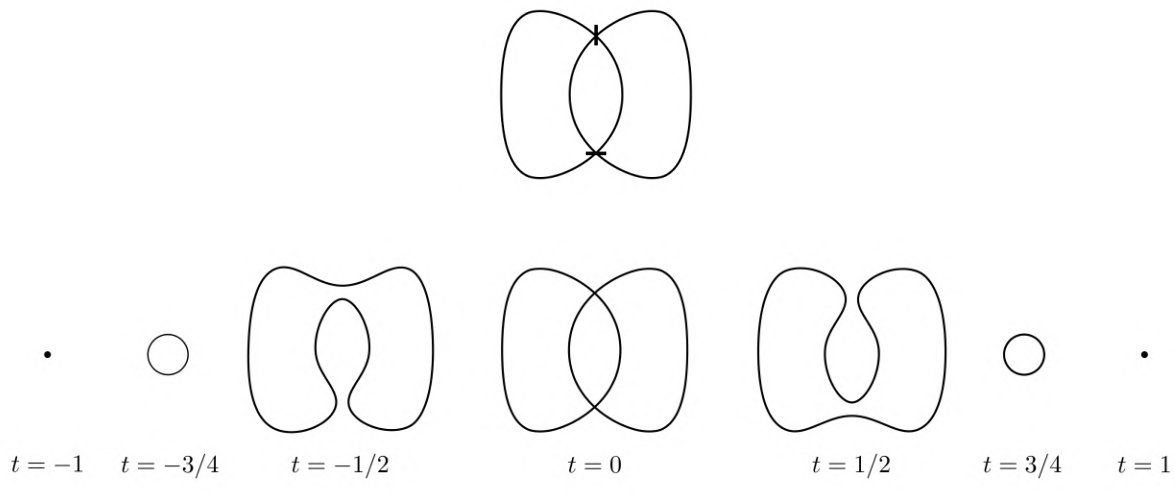

Figure 3.11: A ch-diagram and a motion picture of the hyperbolic splitting of the unknotted torus.

Definition 3.29. We can map a ch-link to an ab-surface (up to $ab3$-moves) through the *thickening map* $\mathfrak{th} : \mathcal{L} \to \mathcal{AB}/ab3$ as defined in Figure 3.13. Since this map is defined on and around marked saddle points, it is a locally defined map. We extend it to the entire ab-surface by glueing the loose edges around a thickened saddle point in such a way that respects the a/b-labelling, which can be done up to $ab3$ moves.

Remark. For $L \in \mathcal{L}$, we have that $L_+ = \partial_a(\mathfrak{th}(L))$ and $L_- = \partial_b(\mathfrak{th}(L))$. As such, we may think of the a/b labels signifying the links "above" and "below" the $t = 0$ hyperplane.

Following this, we may recover the surface knot corresponding to an ab-surface by taking cones over its (trivial) boundary links through

$$\mathfrak{cap} : \mathcal{AB} \to {}^{\{\text{Surface knots}\}}\!/_{\cong}.$$

Consider an ab-surface $B \in \mathcal{AB}$ such that $\partial_a B, \partial_b B \subset \mathbb{R}^3 \times \{0\}$. We consider disjoint unions of embedded disks

$$\{D_a^i\}_i \subset \mathbb{R}^3 \times \{1\},$$
$$\{D_b^j\}_j \subset \mathbb{R}^3 \times \{-1\},$$

laying above and below $t = 0$ satisfying $p_1(\bigcup_i D_a^i) = \partial_a B$ and $p_1(\bigcup_j D_b^j) = \partial_b B$. Then, the union

$$B \cup \bigcup_i D_a^i \cup \bigcup_j D_b^j \cup (\partial_a B \times [0,1]) \cup (\partial_b B \times [-1,0]),$$

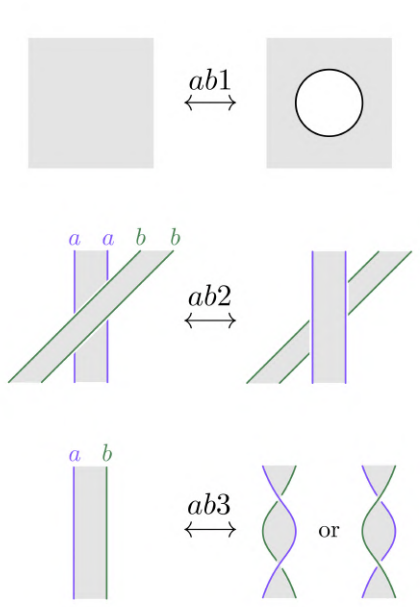

Figure 3.12: ab-moves on ab-surfaces. We remark that the boundary created by the move $ab1$ (colored in black) may be freely labeled with either an a- or b-label.

forms a surface link. We consider $\mathfrak{cap}(B)$ as this surface link (up to ambient isotopy), and note that it is independent of our choice of disk systems $\{D_a^i\}$ and $\{D_b^j\}$. This follows as two trivial disk systems with the same boundary (i.e. either $\partial_a B$ or $\partial_b B$) are ambient isotopic in $\mathbb{R}^3 \times \{-1, 1\}$ [Kam02, ch. 8.5].

We elaborate that the definition of $\mathfrak{cap}$ justifies the move $ab1$; puncturing the ab-surface and labelling the boundary freely does not change the resulting surface after applying $\mathfrak{cap}$, as this puncture will simply get filled in again by a disk.

Applying $\mathfrak{th}$ provides some visual insight as to why the Yoshikawa moves Ω_7 and Ω_8 produce equivalent surface knots as illustrated in Figures 3.14 and 3.15, which is usually not immediately evident. Since these moves result in equivalent ab-surfaces, they produce equivalent surface knots after applying $\mathfrak{cap}$.

Example 3.30. To illustrate the additional visual insight ab-surfaces may provide when considering the hyperbolic splitting corresponding to a given ch-diagram as a surface, we take the torus. Consider Figure 3.16, which shows how an ab-surface of the torus can be acquired from its ch-diagram; first applying $\mathfrak{th}$ to the marked saddle points, and then glueing the loose edges in such a manner that respects the a/b-labelling.

Then, view the boundary links corresponding to the a- and b-labels in $\mathbb{R}^3$ from a different angle as in Figure 3.18a. In this way, we indeed see that the ab-surface presented in Figure 3.18b is diffeomorphic to that in 3.16. To elaborate on why these two ab-surfaces are diffeomorphic, consider Figure 3.17 which illustrates how to deform one of the boundary links.

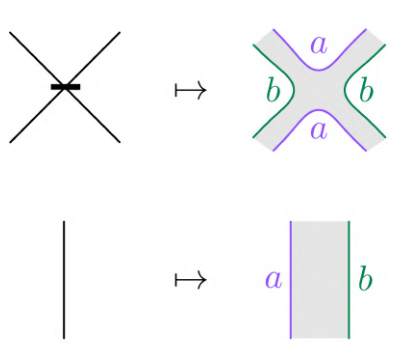

Figure 3.13: The thickening map $\mathfrak{th} : \mathcal{L} \to \mathcal{AB}/ab3$.

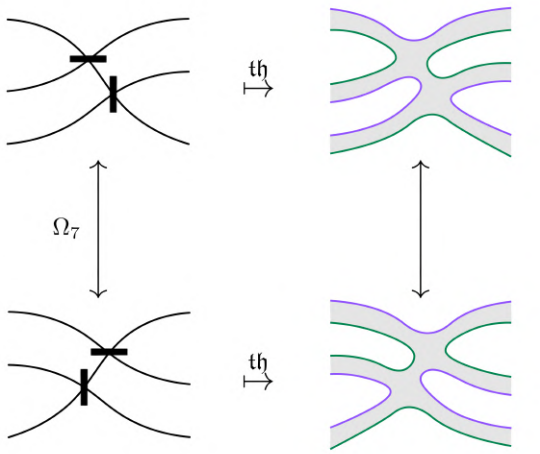

Figure 3.14: Illustrating the Yoshikawa move Ω_7 through the thickening map. The unlabelled arrow on the right-hand side indicates a diffeomorphism.

Coning over each of the boundary links results in the surfaces seen in Figure 3.19. Combining these coned links together with the ab-surface in Figure 3.18b results in the surface in Figure 3.20, from which it becomes evident this surface is indeed the usual torus (in $\mathbb{R}^4$) when taking note of the two holes in the ab-surface. △

In addition to providing a helpful tool for reconstructing a surface from a given ch-diagram, ab-surfaces also play a crucial role in the proof of Theorem 4.7.

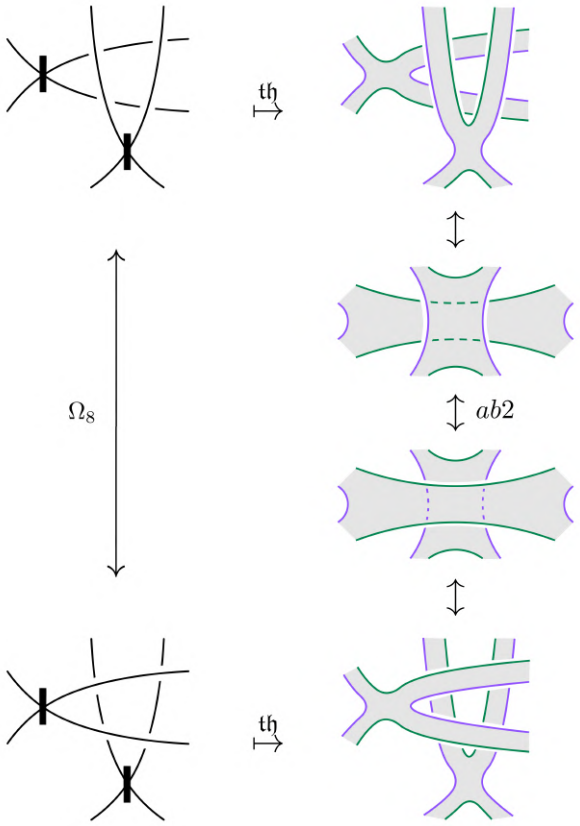

Figure 3.15: Illustrating the Yoshikawa move Ω_8 through the thickening map. The unlabelled arrows on the right-hand side indicate a diffeomorphism.

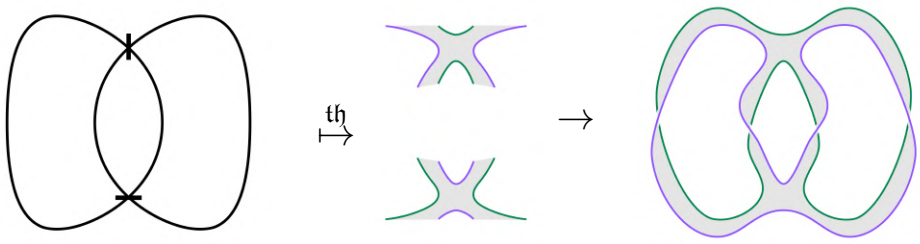

Figure 3.16: Mapping a ch-diagram of the torus to its ab-surface.

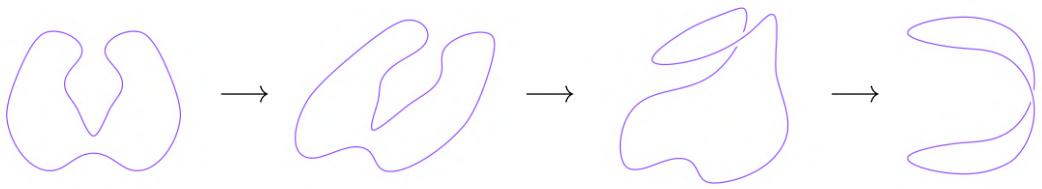

Figure 3.17: Illustrating how to deform the boundary link of the *ab*-surface of the torus.

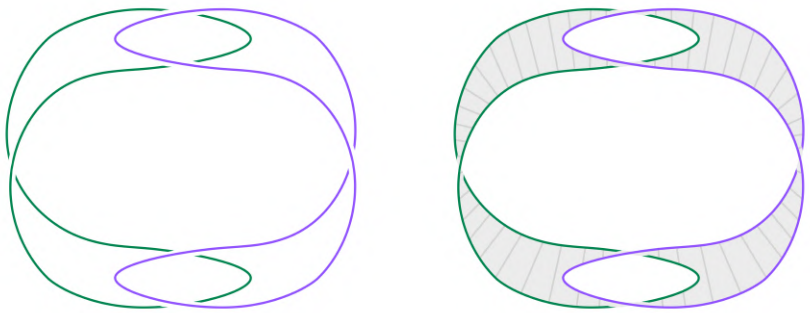

(a) (b)

Figure 3.18: A different view of the *ab*-surface presented in Figure 3.16 (right) and corresponding boundary link (left).

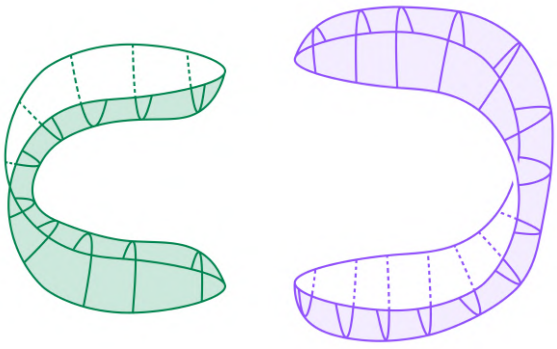

Figure 3.19: Coning over the boundary links of the *ab*-surface of the torus.

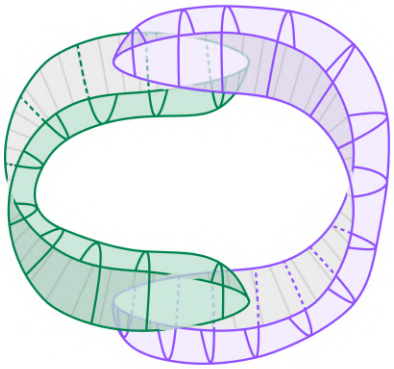

Figure 3.20: A realization of the standard torus in $\mathbb{R}^4$ as constructed from its ch-diagram through means of an *ab*-surface.

3.4 (Twist-)spun knots

In this section, we discuss a way to explicitly construct 2-knots from a given classical knot. The concept of higher dimensional knots was first introduced in 1925 in [Art25] through the so-called spinning construction. We follow the definition as given in [Rol03, ch. 3.J] and [SS98, ch. 1.6]. Define the upper half space $\mathbb{R}^3_+ := \{(x, y, z, 0) \mid z \geq 0\} \subset \mathbb{R}^4$, such that its boundary is $\mathbb{R}^2 = \{(x, y, 0, 0)\}$. The idea of the spinning construction is that we consider an arc A in $\mathbb{R}^3_+$, and that we spin the upper half space with this arc around the boundary $\mathbb{R}^2$ as illustrated in Figure 3.21.

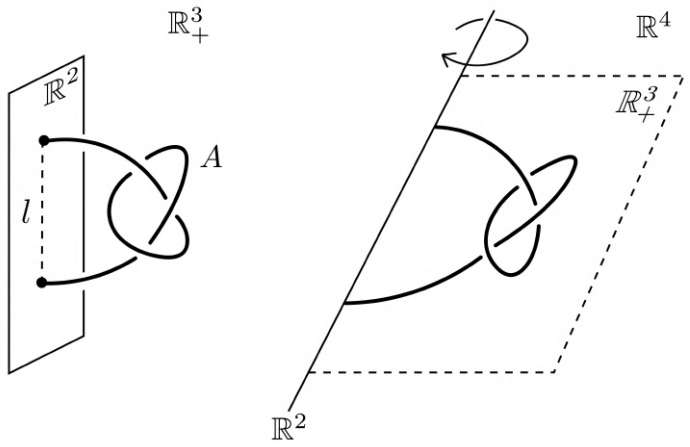

Figure 3.21: The spinning construction for the trefoil knot in $\mathbb{R}^3_+$ and $\mathbb{R}^4$ respectively.

To this end, consider a point $\mathbf{x} = (x, y, z, 0)$ and map it to

$$\mathbf{x}_\theta = (x, y, z\cos\theta, z\sin\theta).$$

Let A be an arc in $\mathbb{R}^3_+$ whose endpoints lie in $\mathbb{R}^2$. The spin of this arc is then given by

$$\text{spun}(A) \coloneqq \{\mathbf{x}_\theta \mid \mathbf{x} \in A,\ \theta \in [0, 2\pi]\}.$$

Let l denote the line segment between the endpoints of A in $\mathbb{R}^2$.

Definition 3.31. If $A \cup l$ forms a classical knot k, then $\text{spun}(k) \coloneqq \text{spun}(A)$ is a 2-knot called the *spun knot obtained from* k. We say l is a *trivial arc* of k.

Notably, k and $\text{spun}(k)$ share many properties. In particular, their knot groups are the same, as shown in Chapter 4.3. An illustration of the spun trefoil is given in Figure 3.22.

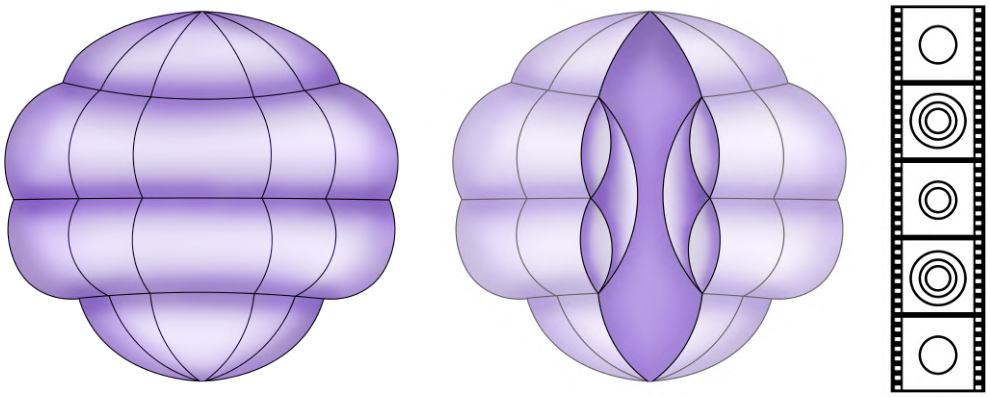

Figure 3.22: The spun knot obtained from the trefoil knot, this same knot with a wedge removed, and the corresponding motion picture.

It turns out ch-diagrams for spun knots of certain classical knots take on a general form (up to stable equivalence) based on the braid part of the classical knot's four-plat, as stated in [All+23, ch. 4] and shown in [MZ15, ch. 5.1]. Figure 3.23 provides this form, to which we remark that the strand without crossings in the four-plat is omitted from "br" in the ch-diagram. This form is thus applicable to all non-trivial prime classical knots as per Lemma 2.12.

Recalling the four-plat of the trefoil and figure-eight knot as in Figure 2.8, we indeed see this general form is consistent with the corresponding spun knots as presented in Table 2, up to stable equivalence.

Spinning two non-equivalent classical knots k_1 and k_2 does not necessarily produce two non-equivalent surface knots $\text{spun}(k_1)$ and $\text{spun}(k_2)$ as shown in [Gor76]. Recall the square knot and granny knot from Figures 2.3d, 2.3e, which

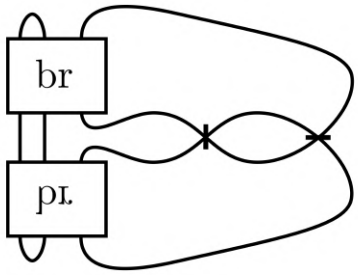

Figure 3.23: The general form of a ch-diagram for certain spun knot, based on the corresponding classical knot's braid description given by br and its mirror image pr, adapted from [All+23, ch. 4].

are known to be non-equivalent. However, their spun knots are equivalent. The result follows when considering the granny as the composition of two trefoil knots, and the square knot as the composition of a trefoil and its mirror image. Figure 3.24 provides an illustration.

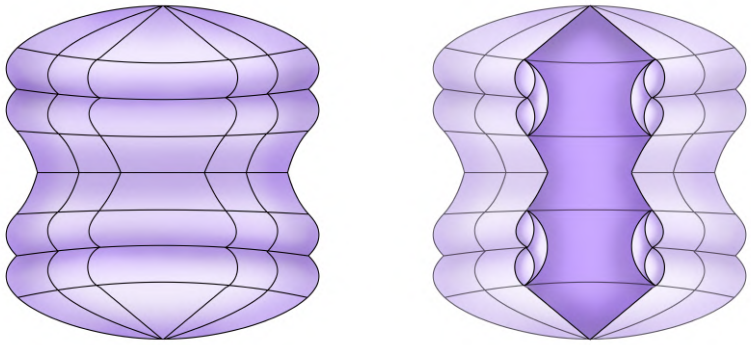

Figure 3.24: The spun knot obtained from the granny or square knot, and this same knot with a wedge removed.

From here, we construct the twist-spun knot, which was originally introduced in [Zee65]. We follow the description as in [Kam02, ch. 10.2], [Kam17, ch. 6.2]. The initial setup is the same as for the usual spun knot as illustrated in Figure 3.21. Assume the knotted part of A lies in a 3-ball $B^3 \subset \mathbb{R}^3_+$, so that $A \cap B^3$ is a knotted arc whose endpoints lie on ∂B^3. Let l' be the middle line of B^3 (parallel to l). Fix an integer m. Let $N(\partial B^3)$ denote a neighbourhood of ∂B^3 in B^3 (so that it is equivalent to a thickened 2-sphere), and denote by B'^3 the closure of the complement of ∂B^3 in B^3 (so that it is equivalent to a smaller ball inside of B^3).

As with regular spinning, we rotate $\mathbb{R}^3_+$ about $\mathbb{R}^2$. While performing this rotation, B^3 is twisted m times about l' as illustrated in Figure 3.25. To this

end, consider the motion

$$\varphi = (\varphi_s \mid s \in [0,1]),$$

of A, such that the restriction of φ_s to B'^3 is a rotation around l' by an angle of $2\pi ms$, the restriction of φ_s to ∂B^3 is the identity, and it is naturally extended to $N(\partial B^3)$.

The motion of twist-spinning is perhaps easier to visualize when we deform A in such a manner that the endpoints of the arc in the 3-ball coincide with the north- and south poles of this ball, i.e. so that $A \cap \partial B^3 = l' \cap \partial B^3$, which may be done without loss of generality. Figure 3.25b provides an illustration.

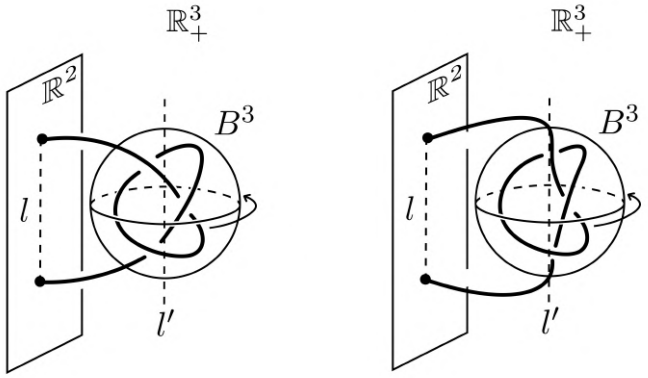

(a) (b)

Figure 3.25: The twist-spinning construction.

Definition 3.32. If $A \cup l$ forms a classical knot k, then the motion φ of A is a 2-knot called the *m-twist-spun knot obtained from k*, denoted by $\text{spun}_m(k)$.

As (twist-)spinning is such an explicit method of producing surface knots, one may expect that the corresponding surfaces are relatively easy to visualize. A visualization of the 2-twist trefoil using modeling software is provided in [Ino13], which also produces a motion picture of the n-twist trefoil. In [LZ22], the authors explore how to effectively generate a motion picture of known surfaces in 4-space with a minimum number of cross-sectional diagrams, which leads to an excellent visualization of the spun trefoil. Figures 3.22 and 3.24 are based on this visualization.

4 The knot group

In this chapter, we discuss how to obtain the knot group of a surface knot through its ch-diagram by generalizing a well-known method for classical knots, the so-called Wirtinger presentation. Additionally, we consider the knot group of (twist-)spun knots, which are closely related to the knot group of the corresponding classical knot.

Definition 4.1. The *knot group* of a surface knot K is the fundamental group of the knot complement, i.e. $\pi_1(\mathbb{R}^4 \setminus K)$, denoted by $G(K)$. Analogously, the knot group of a classical knot k is $\pi_1(\mathbb{R}^3 \setminus k)$, denoted by $G(k)$.

The knot group is an important invariant for both classical and surface knots. If the knot groups of two knots are non-isomorphic, then these knots cannot be equivalent. The converse is not necessarily true, as two inequivalent knots may produce the same knot group. A conjectured exception to this are those 2-knots equivalent to the unknot. If this conjecture proves to be true, the knot group would allow us to distinguish between 2-knots which are knotted and those that are not. A strong argument is provided by Freedman in [Fre84, p. 660], but as stated in [Kam17, ch. 1.2], it remains an open problem to this day.

Conjecture 4.2. *A 2-knot K is unknotted if and only if $G(K) \cong \mathbb{Z}$.*

Remark. For classical knots, it is well known that k is unknotted if and only if $G(k) \cong \mathbb{Z}$ [Kam17, ch. 2.5].

4.1 The Wirtinger presentation

One explicit way of computing a group presentation of the knot group of a classical knot is through its Wirtinger presentation. Before generalizing this method to surfaces, we treat the classical case as to gain a thorough understanding of this presentation. The algorithm and examples presented here are based on [Rol03, ch. 3.D].

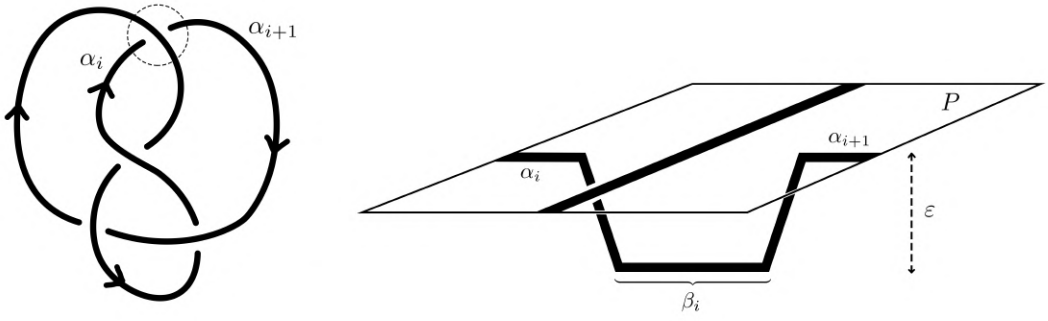

Figure 4.1: Undercrossing β_i connecting α_i to α_{i+1}.

Consider the knot diagram of a classical knot k, and let $\alpha_1, \ldots, \alpha_n$ denote the finite number of arcs that make up the diagram of k. We may assume the α_i lie in any plane, so let us take the x, y-plane $P \coloneqq \{z = 0\}$. Each α_i is connected to $\alpha_{i+1 \mod n}$ by an undercrossing β_i which lies a distance $\varepsilon > 0$ below P, as illustrated in Figure 4.1. In this way, the union of the α_i and these undercrossings form k.

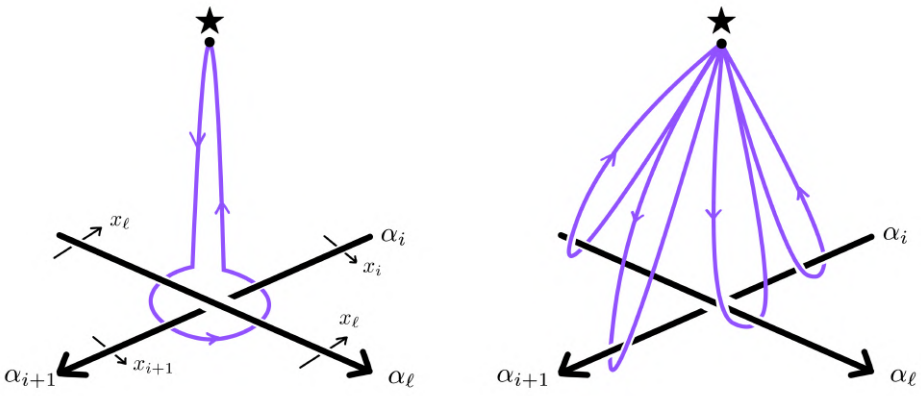

Figure 4.2: Visualizing the loops around a crossing generated by the x_i.

Assign an orientation to the diagram of k which agrees with the order of the α_i, and draw an arrow labelled x_i under each corresponding arc. Take a base point well above P, say $\bigstar \coloneqq (0, 0, 1)$, which is best thought of as the eye of the viewer. The arrows x_i then represent loops in the complement of k consisting of the oriented triangles running from $\bigstar$ to the tail of x_i, along x_i, and from the head of the arrow back to $\bigstar$. See Figure 4.2.

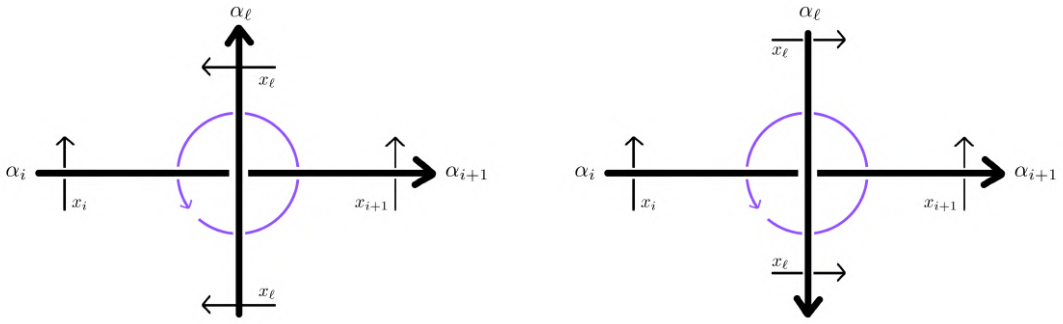

(a) A crossing with relator $x_\ell^{-1} x_{i+1} x_\ell x_i^{-1}$, which is equivalent to the relation

$$r_i : x_\ell x_i = x_{i+1} x_\ell.$$

(b) A crossing with relator $x_\ell x_{i+1} x_\ell^{-1} x_i$, which is equivalent to the relation

$$r_i : x_i x_\ell = x_\ell x_{i+1}.$$

Figure 4.3: On the left, a crossing of type A. On the right, a crossing of type B.

This construction forces a relator in terms of x_i, x_{i+1} and x_ℓ at each crossing, where x_ℓ is the arrow corresponding to the overcrossing arc α_ℓ. The relators at each crossing may take on one of two types as illustrated in Figure 4.3. Typically these relators are written as a relation, so let r_i denote the relation at the undercrossing from α_i to α_{i+1}. As the number of crossings corresponds to the number or arcs of the diagram, this results in n relations $r_1, \ldots, r_n$.

Theorem 4.3 (Wirtinger presentation)**.** *The knot group of k is generated by the arrows and relations as described above, i.e.*

$$G(k) \cong \langle x_1, \ldots, x_n \mid r_1, \ldots, r_n \rangle.$$

Remark. The Wirtinger presentation may be adapted for classical links in the obvious manner by assigning an orientation to each component of the link and then determining the relations from each crossing as usual, as illustrated in Example 4.6.

Before getting into the proof, let us consider a number of examples.

Example 4.4 (Trefoil knot)*.* Consider Figure 4.4. The diagram of the trefoil knot consists of three arcs $\alpha_1, \alpha_2, \alpha_3$, and has corresponding generators x_1, x_2, x_3. All crossings I, II and III are of type B, resulting in the following relations.

$$\begin{aligned} \text{(I)} \quad & r_1 : x_1 x_3 = x_3 x_2, \\ \text{(II)} \quad & r_2 : x_2 x_1 = x_1 x_3, \\ \text{(III)} \quad & r_3 : x_3 x_2 = x_2 x_1. \end{aligned}$$

We see that r_3 is redundant, as we have $x_3 x_2 = x_1 x_3 = x_2 x_1$ by r_1, r_2. We thus have that the knot group of the trefoil knot is isomorphic to

$$\langle x_1, x_2, x_3 \mid x_1 x_3 = x_3 x_2, x_2 x_1 = x_1 x_3 \rangle.$$

Note that r_1 may be rewritten to $x_2 = x_3^{-1} x_1 x_3$, which reduces r_2 to

$$x_3^{-1} x_1 x_3 x_1 = x_1 x_3,$$

or equivalently, $x_1 x_3 x_1 = x_3 x_1 x_3$. The Wirtinger presentation thus reduces to

$$\langle x_1, x_3 \mid x_1 x_3 x_1 = x_3 x_1 x_3 \rangle.$$

△

Example 4.5 (Figure-eight knot)*.* The diagram of the figure-eight knot consists of four arcs $\alpha_1, \ldots, \alpha_4$ and their corresponding generators x_i as in Figure 4.5. Crossings I and III are of type B, while crossings II and IV are of type A, producing the following relations.

$$\begin{aligned} \text{(I)} \quad & r_1 : x_1 x_3 = x_3 x_2, \\ \text{(II)} \quad & r_2 : x_4 x_2 = x_3 x_4, \\ \text{(III)} \quad & r_3 : x_3 x_1 = x_1 x_4, \\ \text{(IV)} \quad & r_4 : x_1 x_2 = x_2 x_4. \end{aligned}$$

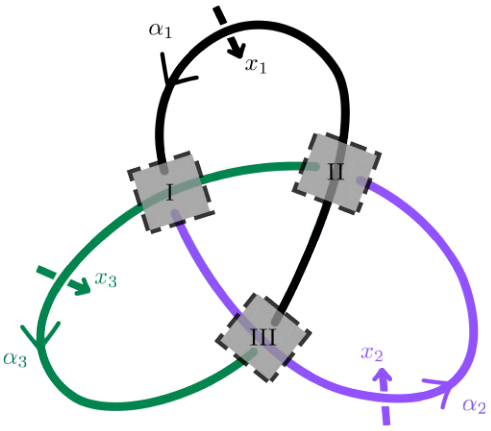

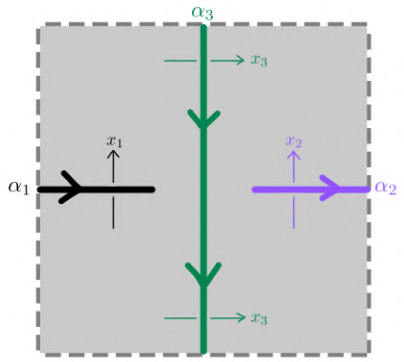

(a) Crossing I

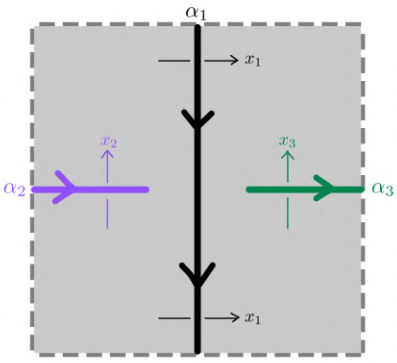

(b) Crossing II

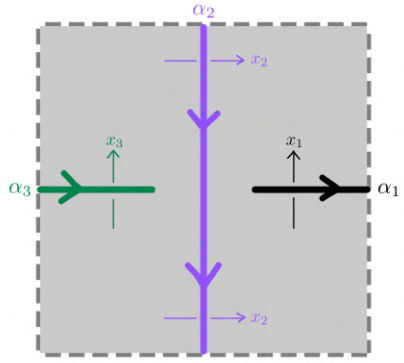

(c) Crossing III

Figure 4.4: Illustrating the Wirtinger presentation for the trefoil knot.

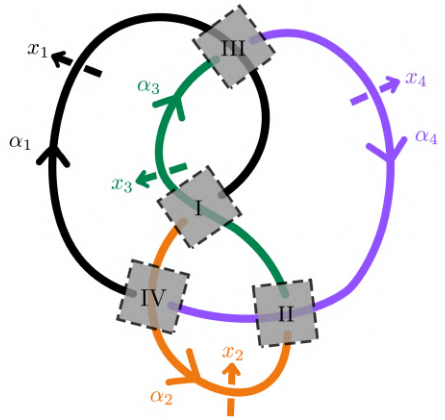

Figure 4.5: Illustrating the Wirtinger presentation for the figure-eight knot.

It turns out r_4 is redundant and follows from the other relations. Write r_1 as $x_2 = x_3^{-1}x_1x_3$, r_2 as $x_3 = x_4x_2x_4^{-1}$, and r_3 as both $x_3 = x_1x_4x_1^{-1}$ and $x_4 = x_1^{-1}x_3x_1$. Then, starting from r_3, we see that

$$\begin{aligned}
\underbrace{x_3}_{r_2} x_1 &= x_1x_4 \\
x_4x_2x_4^{-1}x_1 &= x_1x_4 \\
\underbrace{x_4}_{r_3} x_2 &= x_1x_4x_1^{-1}x_4 \\
x_1^{-1}x_3x_1x_2 &= x_1x_4x_1^{-1}x_4 \\
x_1x_2 &= x_3^{-1}x_1 \underbrace{x_1x_4x_1^{-1}}_{r_3} x_4 \\
x_1x_2 &= \underbrace{x_3^{-1}x_1x_3}_{r_1} x_4 \\
x_1x_2 &= x_2x_4,
\end{aligned}$$

which is indeed r_4.

Using r_1 as $x_2 = x_3^{-1}x_1x_3$ and r_3 as $x_4 = x_1^{-1}x_3x_1$ and substituting them into r_2, we see that

$$\begin{aligned}
x_4x_2 &= x_3x_4, \\
x_1^{-1}x_3x_1x_3^{-1}x_1x_3 &= x_3x_1^{-1}x_3x_1, \\
x_1^{-1}x_3x_1x_3^{-1}x_1x_3x_1^{-1}x_3^{-1}x_1x_3^{-1} &= 1.
\end{aligned}$$

The group presentation thus reduces to

$$\langle x_1, x_3 \mid x_1^{-1}x_3x_1x_3^{-1}x_1x_3x_1^{-1}x_3^{-1}x_1x_3^{-1}\rangle.$$

△

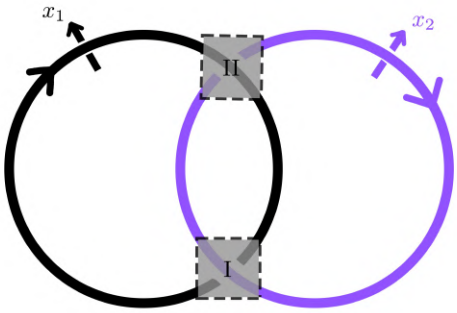

Figure 4.6: Illustrating the Wirtinger presentation for the Hopf link.

Example 4.6 (Hopf link). Consider Figure 4.6. The diagram of the Hopf link consists of two arcs with generators x_1, x_2 after we assign an orientation to both components of the link. Both crossings are of type B, resulting in the relation

$$x_1 x_2 = x_2 x_1,$$

for both crossings. The knot group of the Hopf link is thus isomorphic to

$$\langle x_1, x_2 \mid x_1 x_2 = x_2 x_1 \rangle \cong \mathbb{Z}^2.$$

△

Let us treat the proof of Theorem 4.3.

Proof. As before, consider a classical knot k whose (oriented) diagram lies entirely in P with the exceptions of its undercrossings. The idea of this proof is that we aim to build a structure which is homotopy equivalent the complement of k, so that they have the same fundamental group as per Theorem 2.25. We do so by forming a sort of tube around k and filling up the plane P "outside" of the tube, so that the resulting space is in fact homotopy equivalent to the knot complement when flattening the complement onto P and a neighbourhood of k.

To this end, we broaden each arc α_i in P to be a disk A_i in P. Additionally, the rest of P is filled in with disks D_j inbetween the A_i and D^*, where

$$D^* = P \setminus (\bigcup_j D_j \cup \bigcup_i A_i),$$

so that it covers the area "outside" of the broad knot diagram as in Figure 4.7.

Glue a disk B_i from below to each A_i by identifying two of their sides when considering them as rectangles. We remark that the other two sides are not to be glued, resulting in a sort of tunnel with open ends as illustrated in Figure 4.8. In this way, glueing the B_i produces the generators x_i for the fundamental group of the knot complement by looping from ★ around the tunnel and back to ★ using a right-hand rule, as illustrated in Figure 4.9.

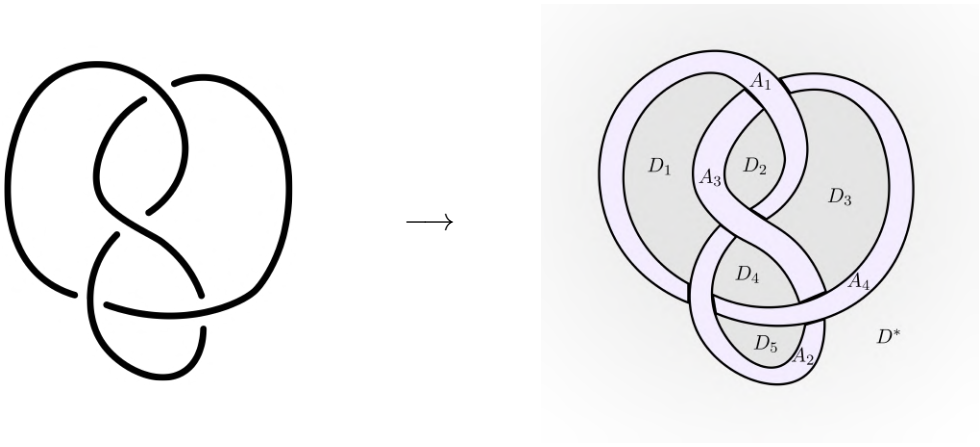

Figure 4.7: Filling up the plane P using disks A_i, D_j and D^*.

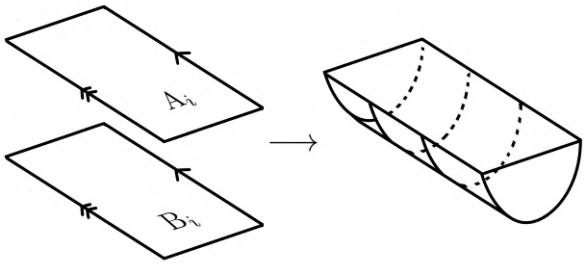

Figure 4.8: Glueing a disk B_i to A_i.

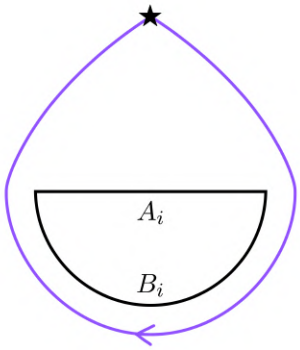

Figure 4.9: A cross section of the complement of k illustrating a loop in this complement generated by glueing a disk B_i to A_i.

The structure we have built so far is homotopy equivalent to the filled up space around the tunnels formed by the union of the α_i without any undercrossings attached, and its fundamental group is thus the free group on the given

generators, i.e. $\langle x_1, \ldots, x_n \mid \varnothing \rangle$.

At each crossing, we now have two open-ended tunnels formed by arcs α_i and α_{i+1} that run into a tunnel formed by α_ℓ, the overcrossing. See Figure 4.10a. To form the undercrossing, we must thus connect the two open-ended tunnels as illustrated in Figure 4.10b. However, we cannot do so directly, as we must make sure not to intersect the tunnel formed by α_ℓ. Thus, we glue a disk (rectangle) R_i in such a way that two of its sides are attached to the bottom of B_ℓ, and the other two are connected to the open sides of B_i and B_{i+1} to complete the undercrossing as seen in Figure 4.11. This forms a connection which functions as an underpass between the α_i and α_{i+1} tunnels, running fully below the α_ℓ tunnel.

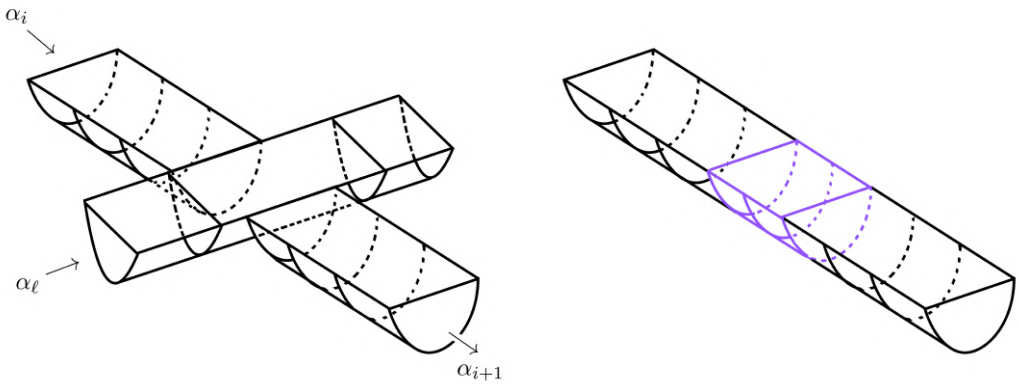

(a) (b)

Figure 4.10: On the left, a neighbourhood of a crossing of k without its under arc installed. On the right, the connection between the tunnels formed by arcs α_i and α_{i+1} we look to install to form the undercrossing.

Glueing such an underpass creates a relation in our group presentation. We thus modify the way the underpass is attached, to make sure this relation is easy to recognize and read off. To achieve this, we widen the underpass to fully span

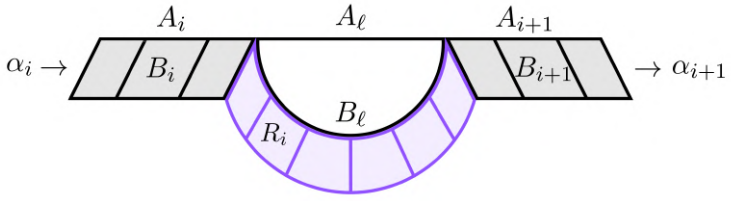

Figure 4.11: A sideview of the underpass between the tunnels formed by α_i and α_{i+1} by glueing a disk R_i.

across the bottom of B_ℓ as illustrated in Figure 4.12. For the relation, walking through the tunnel and then back should be the same as "doing nothing". In this widened tunnel, walking through it and back looks like following the boundary of B_ℓ. As a loop in the complement, this is done similarly to how we illustrated in Figure 4.2. We know how to express this in terms of our generators. For a type A crossing this results in the relation $x_{i+1}x_\ell x_i^{-1}x_\ell^{-1} = 1$, or equivalently $x_\ell x_i = x_{i+1}x_\ell$. For a type B crossing we have $x_{i+1}x_\ell^{-1}x_i^{-1}x_\ell = 1$, or $x_i x_\ell = x_\ell x_{i+1}$. See Figure 4.13.

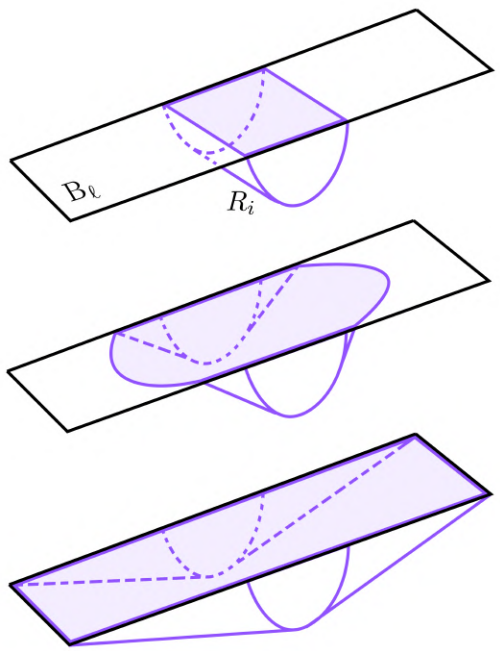

Figure 4.12: Making the underpass (created by glueing R_i) span across the entire bottom of B_ℓ.

Let r_i denote the relation acquired by glueing R_i, and notice that

$$\mathbb{R}^3 \setminus k \simeq \bigcup_i (A_i \cup B_i \cup R_i) \cup \bigcup_j D_j \cup D^*.$$

Consequently, by applying Theorem 2.26 (Seifert-van Kampen) inductively for each glued R_i,

$$\begin{aligned} G(k) = \pi_1(\mathbb{R}^3 \setminus k) &\cong \pi_1\left(\bigcup_i (A_i \cup B_i \cup R_i) \cup \bigcup_j D_j \cup D^*\right) \\ &\cong \langle x_1, \ldots, x_n \mid r_1, \ldots, r_n \rangle, \end{aligned}$$

which completes the proof. □

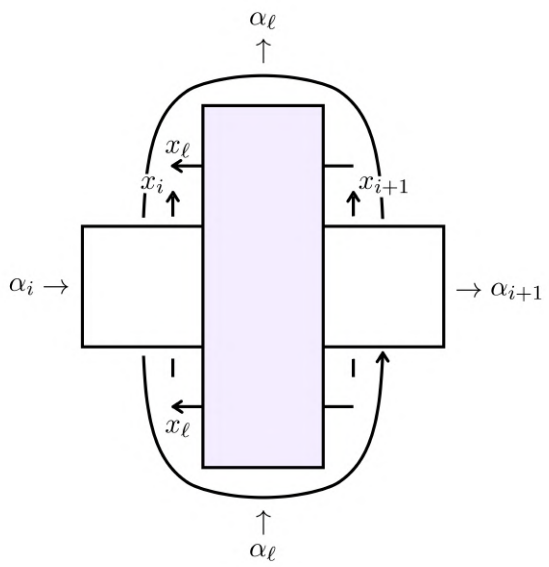

Figure 4.13: Illustrating a loop around a crossing in the neighbourhood of a knot. The pictured crossing is of type A.

4.2 The Wirtinger presentation for surface knots

The usual Wirtinger presentation for classical knots now provides us with a powerful tool for computing the knot group of a surface knot based on its ch-diagram. Assign an orientation to a ch-diagram D of a surface knot K stemming from an orientation of the lower link L_-. Four arcs run into each marked crossing, which are connected in pairs of two following the orientation in L_-. Let x_i be a generator for the first pair, and x_j be a generator for the second pair as illustrated in Figure 4.14. This results in $\mathrm{ch}(K)$-many generators for the whole diagram, as there are $\mathrm{ch}(K)$-many arcs.

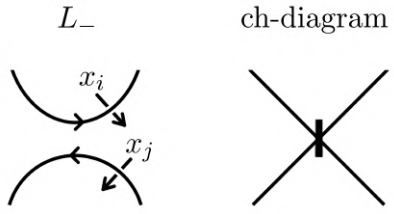

Figure 4.14: Assigning an orientation and corresponding generators based on the lower link L_-.

If an arc directly connects two marked crossings, the number of generators gets reduced by two, as illustrated in Figure 4.15. We denote by a the number of such connections, so that the total number of generators is $\mathrm{ch}(K) - 2a$.

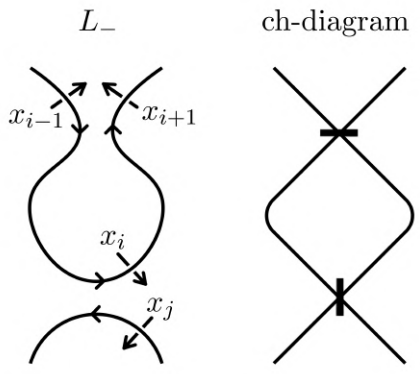

Figure 4.15: When two saddles are directly connected by an arc, the number of generators gets reduced by 2 as $x_{i-1} = x_i = x_{i+1}$ in L_-.

Consider the assigned orientation in L^+; if it is consistent (i.e. does not contradict itself), we acquire a relation $x_i = x_j$. If the orientations do not agree, we have the relation $x_i = x_j^{-1}$. We call this relation r_ℓ^*, and note that there are $h(D)$-many of them as this is the number of marked crossings. When two marked crossings are connected by a direct arc as described above, one of the relations $x_i = x_j$ has already been incorporated into the set of generators. There are thus $(h(D) - a)$-many relations left. We remark that a relation $x_i = x_j^{-1}$ may only occur when the surface link has a non-orientable component.

There are $c(D)$-many crossings in the ch-diagram of K. For each crossing, determine the relation in the same way as for the usual Wirtinger presentation, as described in Figure 4.3. This results in $c(D)$-many relations $r_1, \ldots, r_{c(D)}$.

Theorem 4.7 (Wirtinger presentation for surfaces)**.** *The knot group of K is generated by the generators and relations as described above, i.e.*

$$G(K) \cong \langle x_1, \ldots, x_{\mathrm{ch}(K)-2a} \mid r_1^*, \ldots r_{h(D)-a}^*, r_1, \ldots, r_{c(D)} \rangle.$$

We provide an outline of the proof. Our strategy is similar to that of the proof of the classical Wirtinger presentation (Theorem 4.3), in the sense that we aim to build a neighbourhood of the surface which is homotopy equivalent to the complement of the surface, so that their fundamental groups are the same. The argument consists of two parts; showing that applying the usual Wirtinger presentation to a crossing in a ch-diagram is still justified, and analyzing what relations occur at marked saddle points.

Consider a ch-diagram D of a surface K with arcs α_i, and apply $\mathfrak{th}$ to acquire an *ab*-surface for K. For now, we consider only the parts of the *ab*-surface outside of the saddle areas. Imagine the walls of the *ab*-surface as standing upright (in terms of the z-coordinate, as *ab*-surfaces live in $\mathbb{R}^3$), with the convention that

the a-labelled side lies above. If D lies in $\mathbb{R}^2 \times \{0\}$, then we may see the a- and b-labelled links as lying in $\mathbb{R}^2 \times \{\varepsilon\}$ and $\mathbb{R}^2 \times \{-\varepsilon\}$ respectively, so that the ab-surface is contained in $\mathbb{R}^2 \times [-\varepsilon, \varepsilon]$. Deforming the entire ab-surface in this way is difficult, but as we currently only concern ourselves with the straight edges, we face no issues. Figure 4.16 provides an illustration.

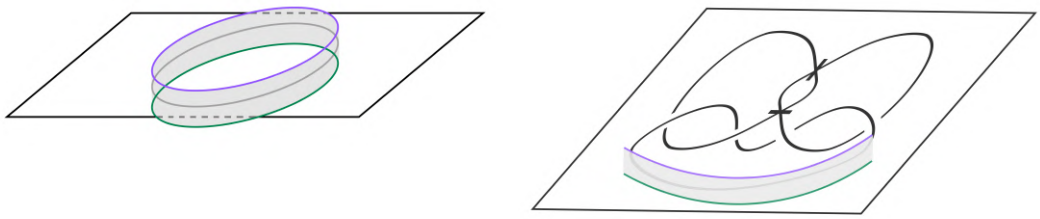

Figure 4.16: Aligning the walls of an ab-surface vertically, illustrated using the unknot and part of the ch-diagram of $6_1^{0,1}$.

From here, product these walls by a unit interval, creating a solid block. This creates an a- and b- labelled side, rather than just an edge. We then identify the remaining two sides to create a tunnel which has thick walls. Note that depending on our choice of visualization, both the a- and b- side may appear as the "inside" lining of this tunnel, meaning it in fact does not matter which label we take on the inside.

We remark that widening the ab-surface and then identifying its sides in this manner is equivalent to producting the ab-surface with $\mathbb{S}^1$ as seen in Figure 4.17. This construction gives us tunnels functioning as a neighbourhood of the ab-surface corresponding to arcs α_i of the ch-diagram. Depending on our choice of visualization, it might occur that the inside of one tunnel segment transforms into the outside of a different tunnel segment, leading to a visual singularity as in Figure 4.18. However, it is important to note that this is not an actual singularity; as both sides function as the inside and outside due to our chosen identification, and the fact that we are working in 4-space, there is no actual intersection happening.

Considering these tunnels around a crossing of D, we see a very similar picture as in the proof of the classical Wirtinger presentation, except this time with thickened walls. See Figure 4.19. Attaching the undercrossings is thus also done in an analogous way by dropping below the tunnel forming the overcrossing, as illustrated in Figure 4.20.

We fill up the rest of $\mathbb{R}^2 \times [-\varepsilon, \varepsilon]$ with solid blocks, and stretch the underpass all the way across the bottom of the overpass as before to simplify the relation acquired by glueing said underpass. This is done entirely analogously as in the classical case (refer to Figure 4.12).

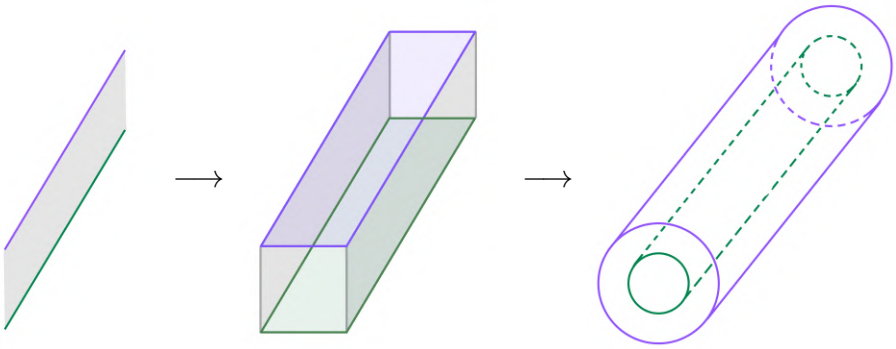

Figure 4.17: Taking a product of the ab-surface with an interval, then identifying the sides of this product.

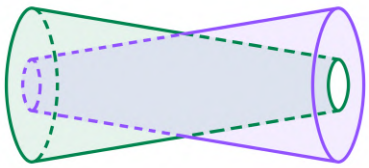

Figure 4.18: A visual singularity.

Recall that applying $\mathfrak{cap}$ to the ab-surface gives us the surface K (up to ambient isotopy), but thus far we have built the complement of the ab-surface before coning over its a- and b-labelled boundary links. However, this does not pose any issues; we may simply product the required disk system with $\mathbb{S}^1$, and then attach it accordingly. The product of a disk with $\mathbb{S}^1$ is a solid torus, which is in line with the a- and b-boundaries of the ab-surface producted with $\mathbb{S}^1$.

Importantly, glueing this system of solid tori (in place of applying $\mathfrak{cap}$) does not affect the group presentation of the tunnel construction as the boundary links of the ab-surface are trivial. The fundamental group of the complement of a solid torus has one generator, and no relations (i.e. it is infinite cyclic). Thus after glueing, no additional relations are added. We may expect to see an additional generator added, but due to the glueing this generator gets "absorbed" by the current set of generators. Under typical circumstances, the process of glueing a solid torus in this manner might result in a new relation, but this is not the case here due to the trivial a- and b- boundary links.

Given that we handle the situation at the saddles appropriately, we can thus conclude that the system of thickened tunnels and the rest of $\mathbb{R}^2 \times [-\varepsilon, \varepsilon]$ being filled up is homotopy equivalent to the complement of the ab-surface in $\mathbb{R}^4$ (by compressing the space in both the t- and z-directions). This means it has the same fundamental group as K, and that the relations at a crossing of D can be read off through the usual process of the Wirtinger presentation.

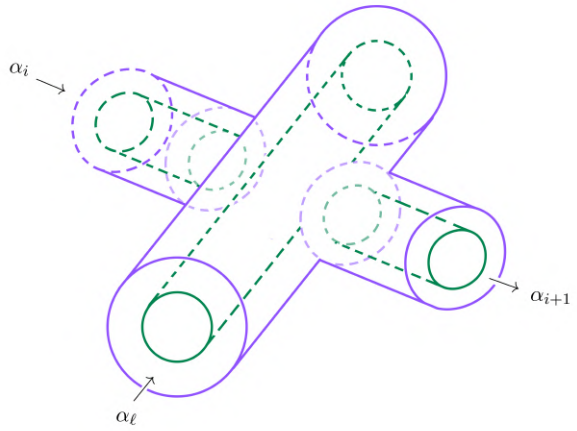

Figure 4.19: The product of an ab-surface with $\mathbb{S}^1$ around a crossing of the ch-diagram, corresponding to arcs α_ℓ, α_i, and α_{i+1}.

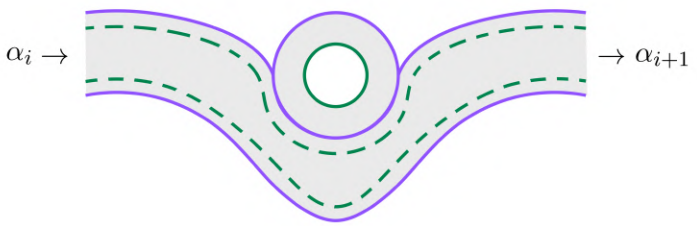

Figure 4.20: Attaching an undercrossing between the tunnels corresponding to arcs α_i and α_{i+1}, from a sideview.

Now for the saddle points. Like with the rest of the ab-surface, we aim to position its walls upright (which is of course not actually possible due to the saddle). As such, we imagine the a-labelled edges corresponding to L_+ as having an upright wall attached to them, and then connect the other edge of the walls in an appropriate way to form the b-labelled edge corresponding to L_-. See Figure 4.21a. One may notice that to do so successfully, we must turn one of the walls "upside down", having the a-labelled edge on the bottom of the wall. However, recall that after producting by $\mathbb{S}^1$ we can see both labels as being on the "inside" or "outside", meaning that this does not pose an issue.

Rather than directly producting with $\mathbb{S}^1$, we revert to our strategy of producting by an interval and then identifying the sides which do not carry an a- or b-label. Figure 4.21b provides an illustration, but visualizing how to identify the sides of the resulting thickened saddle is not easy. However, notice that the centre of a saddle is essentially a solid ball, and the four arcs running out of it are solid blocks (with some of their sides labelled). We can thus ease this visualization somewhat by "inflating" the center ball as done in Figure 4.22.

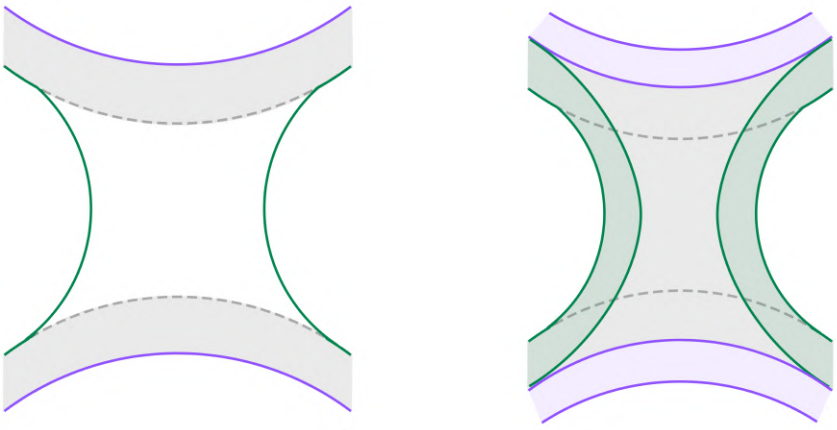

(a) (b)

Figure 4.21: Producting a saddle point of an ab-surface by an interval.

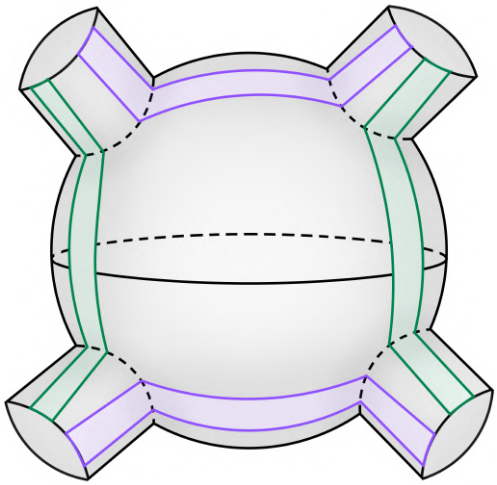

Figure 4.22: Inflating a thickened saddle point.

From here, we notice that after identifying all the non-labelled sides, we acquire tunnels with a- and b-labelled insides all running into each other. It thus follows that the generators corresponding to the four arcs running into the saddle point must agree (up to an inverse to correct for assigned orientation), resulting in the relations r_ℓ^*. We thus indeed get the presentation of the knot group as proposed in Theorem 4.7.

To illustrate Theorem 4.7, we present a few examples.

Example 4.8 ($10_1^{1,1}$). Consider the oriented ch-diagram in Figure 4.23 with generators $x_1, \ldots, x_6$. As per Figure 4.24, the orientation assigned in L_- is consistent when considered in L_+, resulting in the relations

$$x_3 = x_4 = x_5, \quad x_1 = x_2.$$

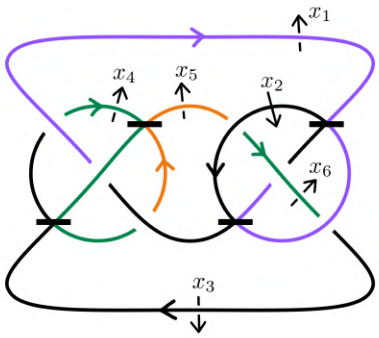

Figure 4.23: Illustrating the Wirtinger presentation for the ch-diagram of $10_1^{1,1}$.

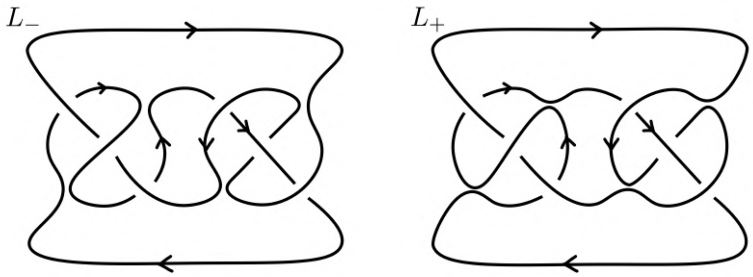

Figure 4.24: Comparing the assigned orientation in L_- to that same orientation in L_+. In this case, the orientations are consistent.

Analyzing the crossings gives us the following relations.

$$\begin{aligned}
&\text{(I)} && x_1x_3 = x_4x_1,\\
&\text{(II)} && x_4x_2 = x_1x_4,\\
&\text{(III)} && x_2x_4 = x_5x_2,\\
&\text{(IV)} && x_1x_6 = x_6x_2,\\
&\text{(V)} && x_6x_1 = x_1x_3,\\
&\text{(VI)} && x_5x_2 = x_2x_6.
\end{aligned}$$

As $x_3 = x_4 = x_5$ and $x_1 = x_2$, this reduces to

$$\begin{aligned}
&\text{(I)} && x_1x_3 = x_3x_1,\\
&\text{(IV)} && x_1x_6 = x_6x_1,\\
&\text{(V)} && x_6x_1 = x_1x_3,\\
&\text{(VI)} && x_3x_1 = x_1x_6,
\end{aligned}$$

or more concisely $x_1x_3 = x_3x_1 = x_1x_6 = x_6x_1$, such that $x_3 = x_6$. We thus get the presentation

$$\langle x_1, x_3 \mid x_1x_3 = x_3x_1\rangle \cong \mathbb{Z}^2.$$

△

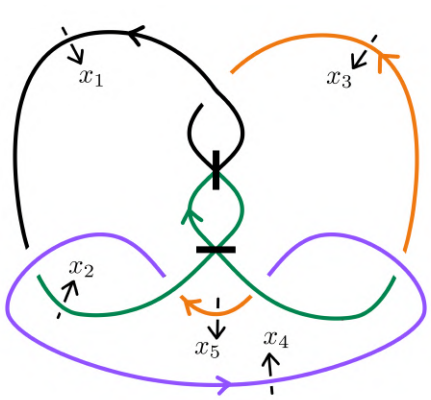

Figure 4.25: Illustrating the Wirtinger presentation for the ch-diagram of $7_1^{0,-2}$.

Example 4.9 ($7_1^{0,-2}$). Consider Figure 4.25 with generators $x_1, \ldots, x_5$. We see from Figure 4.26 that the orientation assigned in L_- is not consistent when considered in L_+, resulting in the relation $x_1 = x_2^{-1}$ We have the following relations.

$$\begin{aligned}
&\text{(I)} && x_3 x_1 = x_1^2,\\
&\text{(II)} && x_1 x_4 = x_4 x_2,\\
&\text{(III)} && x_5 x_2 = x_2 x_4,\\
&\text{(IV)} && x_2 x_4 = x_5 x_2,\\
&\text{(V)} && x_4 x_2 = x_3 x_4.
\end{aligned}$$

Using $x_1 = x_3$ from (I), and $x_1 = x_2^{-1}$, this reduces to

$$\begin{aligned}
&\text{(II)} && x_1 x_4 = x_4 x_1^{-1},\\
&\text{(III)} && x_5 x_1^{-1} = x_1^{-1} x_4,
\end{aligned}$$

which after rewriting results in the group presentation

$$\langle x_1, x_4 \mid x_1 x_4 x_1 x_4^{-1} \rangle.$$

△

Applying Theorem 4.7 to the ch-diagrams in Table 2 results in the list of knot groups as presented in Table 4. Note that the list produced here is consistent with that originally outlined in [Yos94, ch. 5].

Cross-referencing our results against this original list is not always immediate; assigning a different orientation to the ch-diagram may result in differing presentations. In theory, these different presentations should be isomorphic as the fundamental group of the knot complement is not influenced by the orientation we assign to the diagram, but it is not always obvious that this is the case.

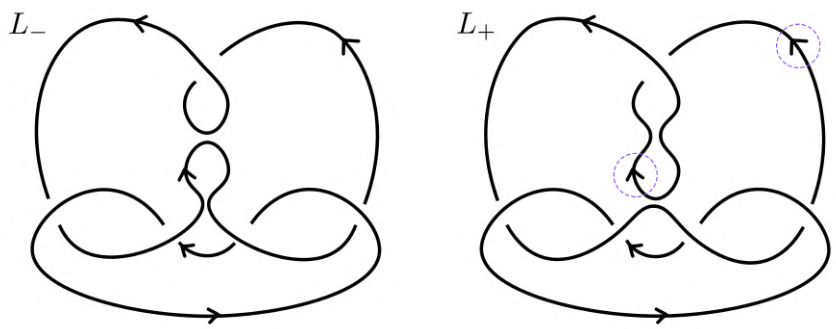

Figure 4.26: Comparing the assigned orientation in L_- to that same orientation in L_+. In this case, the orientations are not consistent, as highlighted on the right-hand side.

Example 4.10. Consider the ch-diagram of 9_1 presented in Table 2 with two different orientations assigned as in Figure 4.27. Let the generators for these oriented ch-diagrams be denoted by x_i and y_i respectively for $i = 1, \ldots, 7$. In both cases the assigned orientation is consistent when considered in L_+, resulting in the relations $x_1 = x_7$ and $y_1 = y_7$.

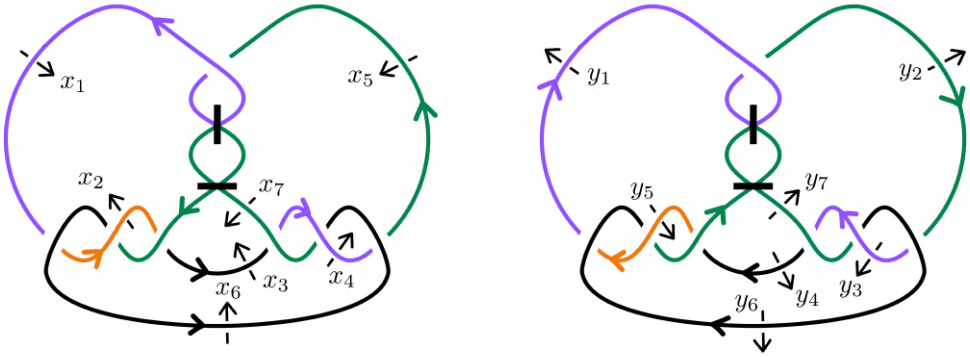

Figure 4.27: A ch-diagram of 9_1 with two different orientations assigned, and their corresponding generators.

For the first case, we get the following relations.

$$\begin{aligned}
&\text{(I)} && x_5x_1 = x_1^2,\\
&\text{(II)} && x_1x_6 = x_6x_2,\\
&\text{(III)} && x_7x_2 = x_2x_6,\\
&\text{(IV)} && x_2x_7 = x_7x_3,\\
&\text{(V)} && x_7x_3 = x_4x_7,\\
&\text{(VI)} && x_4x_6 = x_7x_4,\\
&\text{(VII)} && x_6x_4 = x_5x_6.
\end{aligned}$$

By (I), $x_1 = x_5$. Additionally, notice from (IV) and (V) that $x_2 = x_4$. Reducing by this and $x_1 = x_7$, we have

$$\begin{aligned}
&\text{(II)} && x_1x_6 = x_6x_2,\\
&\text{(III)} && x_1x_2 = x_2x_6,\\
&\text{(IV)} && x_2x_1 = x_1x_3,\\
&\text{(VI)} && x_2x_6 = x_1x_2,\\
&\text{(VII)} && x_6x_2 = x_1x_6.
\end{aligned}$$

Thus, (II) and (VII) are equal, as are (III) and (VI). Rewrite (II) to $x_1 = x_6x_2x_6^{-1}$. Notice from (IV) that x_3 can be expressed fully in terms of x_2 and x_1, and thus in terms of x_2 and x_6, and it does not contribute to any additional relations. We thus get

$$\text{(III)} \qquad x_6x_2x_6^{-1}x_2 = x_2x_6.$$

Multiplying from the right by $(x_6x_2x_6^{-1}x_2)^{-1}$ results in the relator

$$x_2x_6x_2^{-1}x_6x_2^{-1}x_6^{-1},$$

which is equivalent to the relator

$$r \coloneqq x_6x_2^{-1}x_6x_2^{-1}x_6^{-1}x_2.$$

We conclude the group presentation is given by

$$G \coloneqq \langle x_2, x_6 \mid x_6x_2^{-1}x_6x_2^{-1}x_6^{-1}x_2\rangle.$$

In the second case, we get the following relations.

$$\begin{aligned}
&\text{(A)} && y_1^2 = y_1y_2,\\
&\text{(B)} && y_5y_6 = y_6y_1,\\
&\text{(C)} && y_6y_5 = y_5y_7,\\
&\text{(D)} && y_4y_7 = y_7y_5,\\
&\text{(E)} && y_7y_3 = y_4y_7,\\
&\text{(F)} && y_3y_7 = y_6y_3,\\
&\text{(G)} && y_6y_2 = y_3y_6.
\end{aligned}$$

Reducing and rewriting it in the same manner as with the first case, we have that $y_3 = y_5$ and $y_3 = y_6y_1y_6^{-1}$. This results in

$$\text{(C)} \qquad r' \coloneqq y_1y_6^{-1}y_1y_6y_1^{-1}y_6^{-1} = 1,$$

giving the group presentation

$$G' \coloneqq \langle y_1, y_6 \mid y_1y_6^{-1}y_1y_6y_1^{-1}y_6^{-1}\rangle.$$

The two presentations take a very similar form, except that the last and third-to-last elements of the relators have their inverses switched. Are the groups given by these presentations isomorphic? Consider a map defined on the generators of G, given by

$$\begin{aligned}\varphi : G &\to G', \\ x_2 &\mapsto y_5^{-1}, \\ x_6 &\mapsto y_6^{-1}.\end{aligned}$$

It is evident φ is a group homomorphism as it is defined on the generators of G. To see it is well-defined, we show $\varphi(r) = 1$ in G'. Recall that $y_5 = y_3 = y_6 y_1 y_6^{-1}$, from which it follows that

$$\begin{aligned}\varphi(r) &= \varphi(x_6 x_2^{-1} x_6 x_2^{-1} x_6^{-1} x_2) \\ &= y_6^{-1} y_5 y_6^{-1} y_5 y_6 y_5^{-1} \\ &= y_6^{-1}(y_6 y_1 y_6^{-1}) y_6^{-1}(y_6 y_1 y_6^{-1}) y_6 (y_6 y_1^{-1} y_6^{-1}) \\ &= y_1 y_6^{-1} y_1 y_6 y_1^{-1} y_6^{-1} = r' = 1.\end{aligned}$$

To show bijection, consider the inverse of φ given by

$$\begin{aligned}\psi : G' &\to G, \\ y_1 &\mapsto x_1^{-1}, \\ x_6 &\mapsto x_6^{-1}.\end{aligned}$$

To show ψ is well-defined, recall that $x_1 = x_6 x_2 x_6^{-1}$, such that

$$\begin{aligned}\psi(r') &= \psi(y_1 y_6^{-1} y_1 y_6 y_1^{-1} y_6^{-1}) \\ &= x_1^{-1} x_6 x_1^{-1} x_6^{-1} x_1 x_6 \\ &= (x_6 x_2^{-1} x_6^{-1}) x_6 (x_6 x_2^{-1} x_6^{-1}) x_6^{-1} (x_6 x_2 x_6^{-1}) x_6 \\ &= x_6 x_2^{-1} x_6 x_2^{-1} x_6^{-1} x_2 = r = 1.\end{aligned}$$

Thus, G and G' are in fact isomorphic. The presentation for G' is the one provided in [Yos94, ch. 5].

△

4.3 (Twist-)spun knots

The knot groups of (twist-)spun knots are of particular interest as they are closely related to the knot group $G(k)$ of the corresponding classical knot k. Consider the Wirtinger presentation of k

$$G(k) \cong \langle x_1, \ldots, x_n \mid r_1, \ldots, r_{n-1} \rangle,$$

as in Theorem 4.3. The following results then hold as presented in [Kam17, ch. 6.1-2].

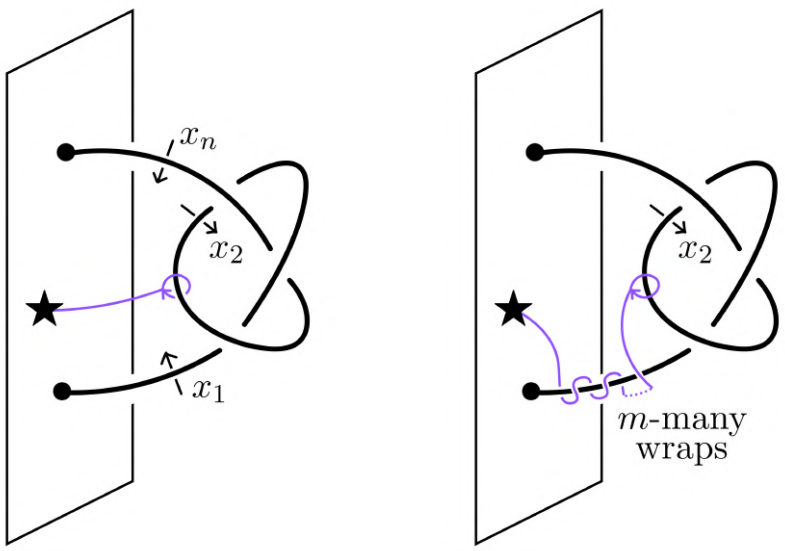

(a) $\theta = 0$ (b) $\theta = 2\pi$

Figure 4.28: A view of m-twist-spinning in $\mathbb{R}^3_+$ at angles $\theta = 0, 2\pi$ to illustrate the relation $x_i = x_1^{-m} x_i x_1^m$. Note that we may also use the generator x_n instead of x_1 as it lies at an end segment of A.

Theorem 4.11. *If $K = \text{spun}(k)$ for some classical knot k, then their knot groups coincide, i.e. $G(K) \cong G(k)$.*

Theorem 4.12. *Consider a classical knot k made up of an arc A and a line segment l as in Definition 3.31. Let x_1 be one of the generators at the endpoints of the arc A as illustrated in Figure 4.28a. If $K = \text{spun}_m(k)$ for some integer m, then its knot group is given by*

$$G(K) \cong \langle x_1, \ldots, x_n \mid r_1, \ldots, r_{n-1}, R \rangle,$$

where R is the set of relations

$$x_i = x_1^{-m} x_i x_1^m \quad (i = 1, \ldots, n).$$

For the proof, we refer to [Zee65]. An intuitive argument presented in [Rol03, ch. 3.L] is as follows. Figure 4.28a depicts a loop with generator x_2 in $\mathbb{R}^3_+ \setminus k$, which corresponds to a loop in $\mathbb{R}^4 \setminus K$. While spinning $\mathbb{R}^3_+$, we ensure this loops stays within $\mathbb{R}^3_+$. As A twists, we must also twist the tail of the loop m times. This leads to a homotopy in $\mathbb{R}^4$ between the loops in Figures 4.28a and 4.28b which does not disturb K. Since the tail of the loop generated by x_2 wraps m times around an end segment of k, we get the relation $x_2 = x_1^{-m} x_2 x_1^m$ for the knot group of K. The same argument may be made for the other arcs of A and

their generators x_i. Thus, the m-th power of x_1 must commute with all other generators $x_1, \ldots, x_n$ of $G(k)$.

We remark that Theorems 4.11 and 4.12 are consistent with the results in Table 4. In particular, 8_1, 10_1, 10_2 and 10_3 are (twist-)spun knots trefoil and figure-eight knot, and their knot groups found through the Wirtinger presentation for surface knots are in line with the aforementioned theorems[8]. This is perhaps somewhat unexpected, as a surface knot may have many presentations of which it is not immediately apparent that they are isomorphic.

Interestingly, it follows (in part) from Theorem 4.12 that every 1-twist-spun knot is a trivial 2-knot as stated in [Kam02, ch. 10.2].

Corollary 4.13. *If $K = \mathrm{spun}_1(k)$ for some classical knot k, then its knot group is infinite cyclic, i.e. $G(K) \cong \mathbb{Z}$.*

Proof. By Theorem 4.12,

$$G(K) \cong \langle x_1, \ldots, x_n \mid r_1, \ldots, r_{n-1}, x_i = x_1^{-1} x_i x_1 \ \ (i = 1, \ldots, n) \rangle.$$

Thus, every conjugate of x_i by x_1 equals itself for $i = 1, \ldots, n$, i.e. they commute. However, we know the relations $r_1, \ldots r_{n-1}$ are all of the form $x_{i+1} = x_\ell x_i x_\ell^{-1}$ or $x_{i+1} = x_\ell^{-1} x_i x_\ell$ by construction of the Wirtinger presentation. As x_1 commutes with each x_i, it follows that all generators x_i of the presentation collapse to just one generator, resulting in

$$G(K) \cong \langle x_1 \mid \varnothing \rangle \cong \mathbb{Z}.$$

□

Recalling Conjecture 4.2, we know Corollary 4.13 alone is not sufficient to state that every 1-twist-spun knot is unknotted. However, [Zee65, ch. 6] provides a full proof of this fact.

[8]For the knot group of the trefoil and figure-eight knot, refer to Examples 4.4 and 4.5

5 Discussion and further research

To summarize, this thesis investigates surface knots with a particular focus on 2-knots. Several visualization methods are introduced, including motion pictures, ch-diagrams, and *ab*-surfaces. We discuss and proof the Wirtinger presentation for classical knots, which allows us to determine the knot group of a classical knot. We generalize this method to surface knots by applying the algorithm to ch-diagrams. To this end, a proof sketch using *ab*-surfaces is outlined. The results of this method are cross-referenced with the results outlined in [Yos94] to confirm its consistency and correctness. A particular type of 2-knot appears repeatedly in our analysis, namely the (twist-)spun knot of a given classical knot; (twist-)spinning gives us a very concrete method of constructing a surface knot, and the knot group of the resulting surface is closely related to that of the corresponding classical knot. Many illustrations and examples are provided throughout the text to help solidfy our understanding of the presented concepts.

Let us consider some possible directions for further research related to the topics presented in this thesis. First and foremost, an important tool for analyzing surface knots is not treated in this text, namely the so-called *broken surface diagrams*. These diagrams are in some sense analogous to knot diagrams for classical knots, as they are a generic projection equipped with over- and undercrossing information at each double curve, which is typically indicated by removing an open neighbourhood from the lower curve. For details, we refer to [Kam17, ch. 4].

There exists a set of moves on these broken surface diagrams called *Roseman moves*, and two surfaces knots are equivalent if and only if their broken surface diagrams are related by Roseman moves and ambient isotopies of $\mathbb{R}^3$ [Kam17, ch 4.2]. It is shown in [Cht24] that Yoshikawa moves follow from Roseman moves through use of *ab*-surfaces, leading to an alternative proof of Theorem 3.14 than the one originally presented in [Swe01]. It is worth exploring the converse, i.e. whether Roseman moves may also be deduced from Yoshikawa moves.

The ch-diagrams in Table 2 are directly adapted from [Yos94], but it would be valuable to study how to explicitly construct these ch-diagrams, and expanding the table for surfaces of ch-index greater than 10. We briefly touch on explicit construction in Figure 3.23 for a particular type of spun knot. Intuitively, the construction provided here relies on the strand closest to the spinning plane not having any crossings, which allows it to smoothly sweep out a double saddle point. This forces all other critical points to be maxima and minima. Taking the cross section at $t = 0$ then clearly results in this double saddle, and two mirrored copies of the braid. Perhaps a good first step would be generalizing this ch-diagram for spun knots to classical knots which cannot (necessarily) be expressed as a four-plat.

A particular point of improvement in this thesis is the lack of a full and rigorous proof of Theorem 4.7, i.e. the Wirtinger presentation for surfaces. The suggested approach should be worked out in more detail, but other strategies are

also worth exploring. One possibility is described in [Fox62, ch. 6] and [BW03, ch. 6.2] by considering $\mathbb{R}^4$ to be made up of a set of boxes (in terms of the t-coordinate), each containing one critical point. This method may perhaps be adapted so that the box at $t = 0$ contains only the ch-diagram, and all other rectangles contain only minima or maxima, which lead to the relations r_ℓ^* in Theorem 4.7.

A different Wirtinger presentation for surface knots using broken surface diagrams is presented in [Yaj62] and [SS98, ch. 5.2], which was later simplified in [Kam01]. Combining this method with the tools in [Cht24] can perhaps result in an effective proof for the Wirtinger presentation on ch-diagrams.

A class of surface knots not considered throughout this text are those surfaces which are not locally flat. A notable example of such surfaces are *suspension knots*. Suspension is another method of forming a surface knot from a given classical knot, and was introduced simultaneously as spun knots in [Art25]. For details on suspension knots, and an analysis on their knot group (which is always trivial), we refer to [AC59].

This thesis focuses only on a limited number of surface knot invariants, namely the ch-index and knot group, but many other well-known invariants exist. A number of such invariants are studied extensively in [Kam17], including (but not limited to) normal Euler number (ch. 3.7, 4.4), elementary ideals and the Alexander polynomial (ch. 3.8), and quandle homology groups (ch. 9).

In the same way we have generalized classical knots to 2-knots by knotting a 2-sphere instead of $\mathbb{S}^1$, we may generalize to arbitrary n-knots which are surfaces in $\mathbb{R}^{n+2}$ homeomorphic to $\mathbb{S}^n$. An explicit construction for a certain kind of n-knot is given in [FI24], which discusses the twist-spinning of twist-spun knots of classical knots. The Wirtinger presentation also extends to n-knots as shown in [Kea75] using critical level embeddings. Many well-known concepts in classical and surface knot theory may generalize or have analogues in n-knot theory, a direction worthy of future research.

Given the modern-day technology, another avenue to consider is that of (computer-assisted) visualization methods, elaborating on the work of e.g. [LZ22] and [Ino13]. An excellent example of the development of such a method is provided in [Sat02], which describes how to build a broken surface diagram of a twist-spun knot.

Appendix A. Tables

0_1 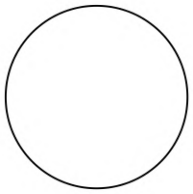	2_1^1 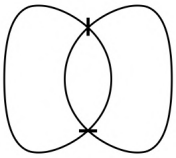	2_1^{-1} 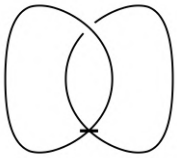
$6_1^{0,1}$ 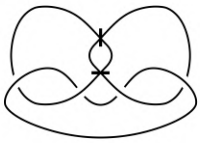	$7_1^{0,-2}$ 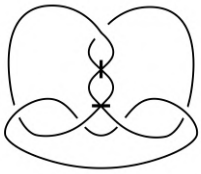	
8_1 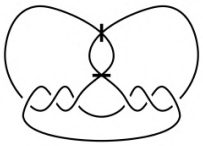	$8_1^{1,1}$ 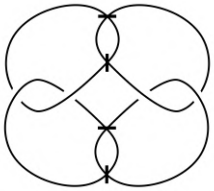	$8_1^{-1,-1}$ 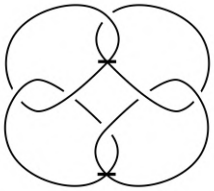
9_1 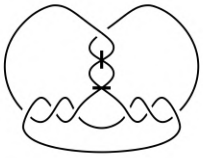	$9_1^{1,-2}$ 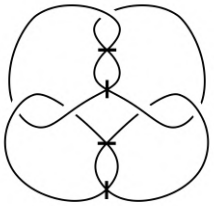	$9_1^{0,1}$ 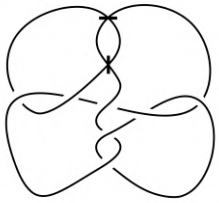
10_1 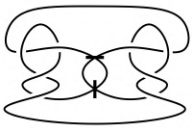	10_2 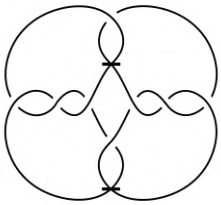	10_3 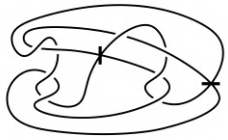
$10_1^{0,1}$ 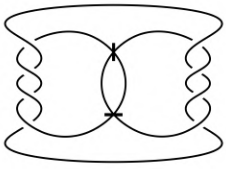	$10_2^{0,1}$ 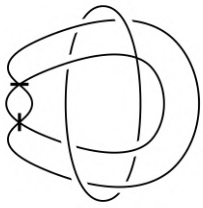	10_1^1 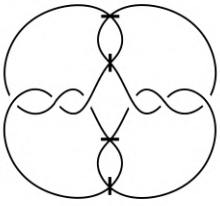

$10_1^{0,-2}$ 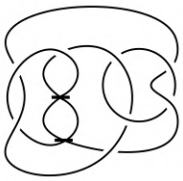	$10_2^{0,-2}$ 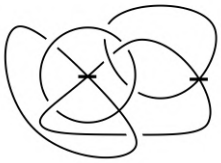	$10_1^{-2,-2}$ 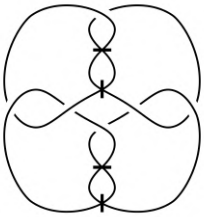
$10_1^{1,1}$ 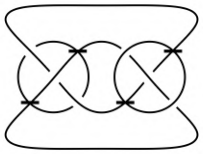	$10_1^{-1,-1}$ 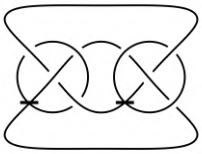	$10_1^{0,0,1}$ 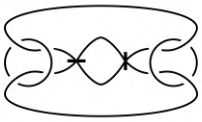

Table 2: Ch-diagrams of all weakly prime surface links with ch-index up to 10.

$I_\ell^{g_1,\ldots,g_c}$	Description	Category
0_1	Unknot	2-knot
2_1^1	Unknotted torus	T^2-knot
2_1^{-1}	Unknotted projective plane	P^2-knot
8_1	Spun knot of trefoil knot	2-knot
$8_1^{1,1}$	Spun surface of Hopf link	Surface link
9_1	Ribbon surface knot[9]of the Stevedore knot	2-knot
10_1	Spun knot of figure-eight knot	2-knot
10_2	2-twist-spun knot of trefoil knot	2-knot
10_3	3-twist-spun knot of trefoil knot	2-knot
10_1^1	Spun torus of the trefoil knot	T^2-knot
$10_1^{1,1}$	1-twist-spun surface of Hopf link	Surface link

Table 3: A brief description of a number of surfaces listed in Table 2.

[9]For an introduction to ribbon knots, we refer to [Kam17, ch 5.5].

K	$G(K)$
0_1	$\mathbb{Z}$
2_1^1	$\mathbb{Z}$
2_1^{-1}	$\mathbb{Z}_2$
$6_1^{0,1}$	$\mathbb{Z}^2$
$7_1^{0,-2}$	$\langle x_1, x_2 \mid x_1x_2x_1x_2^{-1}\rangle$
8_1	$\langle x_1, x_2 \mid x_1x_2x_1 = x_2x_1x_2\rangle$
$8_1^{1,1}$	$\mathbb{Z}^2$
$8_1^{-1,-1}$	Quaternion group
9_1	$\langle x_1, x_2 \mid x_1x_2^{-1}x_1x_2x_1^{-1}x_2^{-1}\rangle$
$9_1^{1,-2}$	$\langle x_1, x_2 \mid x_2x_1x_2x_1^{-1}\rangle$
$9_1^{0,1}$	$\langle x_1, x_2 \mid x_1^{-1}x_2^{-1}x_1x_2x_1^{-1}x_2x_1x_2^{-1}\rangle$
10_1	$\langle x_1, x_2 \mid x_1^{-1}x_2x_1x_2^{-1}x_1x_2x_1^{-1}x_2^{-1}x_1x_2^{-1}\rangle$
10_2	$\langle x_1, x_2 \mid x_1x_2x_1x_2^{-1}x_1^{-1}x_2^{-1},\ x_1^{-2}x_2x_1^2x_2^{-1}\rangle$
10_3	$\langle x_1, x_2 \mid x_1x_2x_1x_2^{-1}x_1^{-1}x_2^{-1},\ x_1^{-3}x_2x_1^3x_2^{-1}\rangle$
$10_1^{0,1}$	$\langle x_1, x_2 \mid x_1^{-1}x_2^{-1}x_1^{-1}x_2x_1x_2x_1x_2^{-1}\rangle$
$10_2^{0,1}$	$\langle x_1, x_2 \mid x_1^2x_2x_1^{-2}x_2^{-1}\rangle$
10_1^1	$\langle x_1, x_2 \mid x_1x_2x_1 = x_2x_1x_2\rangle$
$10_1^{0,-2}$	$\langle x_1, x_2 \mid x_1^{-1}x_2^{-1}x_1x_2x_1^{-1}x_2x_1x_2\rangle$
$10_2^{0,-2}$	$\langle x_1, x_2, x_3 \mid x_1x_2x_1^{-1}x_3^{-1},\ x_2^2 = x_3^2 = (x_2x_3)^2\rangle$
$10_1^{-2,-2}$	Quaternion group
$10_1^{1,1}$	$\mathbb{Z}^2$
$10_1^{-1,-1}$	Dic_4, the dicyclic group of 16 elements
$10_1^{0,0,1}$	$\langle x_1, x_2, x_3 \mid x_2^{-1}x_1^{-1}x_3x_1x_2x_3^{-1}\rangle$

Table 4: The knot groups of the surfaces listed in Table 2.

References

[AC59] J. Andrews and M. Curtis. "Knotted 2-spheres in the 4-sphere". In: *Annals of Mathematics* 70.3 (1959), pp. 565–571. DOI: 10.2307/1970330.

[Ada04] C. Adams. *The knot book: an elementary introduction to the mathematical theory of knots*. American Mathematical Society, 2004. ISBN: 978-0-8218-3678-1.

[All+23] W. Allred et al. "Tri-plane diagrams for simple surfaces in S^4". In: *arXiv* (2023). URL: https://arxiv.org/pdf/2302.08431v1.

[Art25] E. Artin. "Zur Isotopie zweidimensionaler Flächen im R4". In: *Abhandlungen des Mathematischen Seminars der Universität Hamburg* 4 (1925), pp. 174–177. DOI: 10.1007/BF02950724.

[BW03] J. Boersema and E. Whitaker. "Knots in Four Dimensions and the Fundamental Group". In: *Rose-Hulman Undegraduate Mathematics Journal* 4.2 (2003). URL: https://scholar.rose-hulman.edu/rhumj/vol4/iss2/2.

[Cht24] O. Chterental. "Yoshikawa moves on marked graphs via Roseman's Theorem". In: *arXiv* (2024). URL: https://arxiv.org/abs/1701.07170.

[DF03] D. Dummit and R. Foote. *Abstract Algebra, third edition*. John Wiley and Sons, Inc., 2003. ISBN: 978-0471433347.

[FI24] M. Fukuda and M. Ishikawa. "Twist spun knots of twist spun knots of classical knots". In: *arXiv* (2024). URL: https://arxiv.org/abs/2409.00650.

[Fox62] R. Fox. "A quick trip through knot theory". In: *Topology of 3-Manifolds and Related Topics (Proceedings of The University of Georgia Institute, 1961)*. Ed. by M. Fort Jr. Prentice-Hall, Englewood Cliffs, 1962, pp. 120–167.

[Fre84] M. Freedman. "The disk theorem for four-dimensional manifolds". In: *Proceedings of the International Congress of Mathematicians*. Ed. by Z. Ciesielski and C. Olech. Polish Scientific Publishers, 1984, pp. 647–663.

[Gor76] C. M. Gordon. "A note on spun knots". In: *Proceedings of the American Mathematical Society* 58 (1976), pp. 361–362.

[Hat01] A. Hatcher. *Algebraic Topology*. Cambridge University Press, 2001. ISBN: 978-0-521-79540-1. DOI: 10.1017/S0013091503214620.

[Ino13] A. Inoue. "A Symmetric Motion Picture of the Twist-Spun Trefoil". In: *Experimental Mathematics* 22.1 (2013), pp. 15–25. DOI: 10.1080/10586458.2013.748310.

[Kam01] S. Kamada. "Wirtinger presentations for higher dimensional manifold knots obtained from diagrams". In: *Fundamenta Mathematicae* 168 (2001), pp. 105–112. DOI: 10.4064/fm168-2-1.

[Kam02] S. Kamada. *Braid and Knot Theory in Dimension Four*. American Mathematical Society, 2002. ISBN: 978-0821829691.

[Kam17] S. Kamada. *Surface-Knots in 4-space*. Springer, 2017. ISBN: 978-981-10-4090-0. DOI: 10.1007/978-981-10-4091-7.

[Kam89] S. Kamada. "Nonorientable surfaces in 4-space". In: *Osaka Journal of Mathematics* 26.2 (1989), pp. 367–385. URL: https://projecteuclid.org/journals/osaka-journal-of-mathematics/volume-26/issue-2/Nonorientable-surfaces-in-4-space/ojm/1200781549.full.

[Kea75] C. Kearton. "Presentations of n-Knots". In: *Transactions of the American Mathematical Society* 202 (1975), pp. 123–140. URL: https://www.ams.org/journals/tran/1975-202-00/S0002-9947-1975-0358795-1/S0002-9947-1975-0358795-1.pdf.

[KSS82] A. Kawauchi, T. Shibuya, and S. Suzuki. "Descriptions on surfaces in four-space. I. Normal forms." In: *Mathematics Seminar Notes* 10.1 (1982), pp. 75–125. URL: https://www.researchgate.net/publication/268176987.

[Lee13] J. Lee. *Introduction to Smooth Manifolds*. Springer, 2013. ISBN: 978-1-4419-9981-8. DOI: 10.1007/978-1-4419-9982-5.

[LZ22] H. Liu and H. Zhang. "A Flip-book of Knot Diagrams for Visualizing Surfaces in 4-Space". In: *Computer Graphics Forum* 41.3 (2022), pp. 345–354. DOI: 10.1111/cgf.14545.

[Mil63] J. Milnor. *Morse Theory*. Princeton University Press, 1963. ISBN: 978-0691080086.

[Mun14] J. Munkres. *Topology*. Pearson, 2014. ISBN: 978-1-292-02362-5.

[MZ15] J. Meier and A. Zupan. "Bridge trisection of knotted surfaces in S^4". In: *arXiv* (2015). URL: https://https://arxiv.org/pdf/1507.08370.

[nLa25] nLab. *Plat closure*.
https://ncatlab.org/nlab/show/plat+closure.
Accessed on October 30th, 2025. 2025.

[Rol03] D. Rolfsen. *Knots and Links*. AMS Chelsea Publishing, 2003.
ISBN: 9780821834367.

[RS82] C. Rourke and B. Sanderson.
Introduction to Piecewise-Linear Topology. Springer, 1982.
ISBN: 978-3-540-111102-3. DOI: 10.1007/987-3-64281735-9.

[Sat02] S. Satoh. "Surface diagrams of twist-spun 2-knots". In: *Journal of Knot Theory and Its Ramifications* 11.3 (2002), pp. 413–440.
DOI: 10.1142/S0218216502001718.

[SS98] J. Scott Carter and M. Saito. *Knotted Surfaces and Their Diagrams*.
American Mathematical Society, 1998. ISBN: 0-8218-0593-2.
DOI: 10.1090/surv/055.

[Swe01] F. Swenton. "On a calculus for 2-knots and surfaces in 4-space".
In: *Journal of Knot Theory and its Ramifications* 10.8 (Dec. 2001),
pp. 1133–1141. DOI: 10.1142/S0218216501001359.

[Yaj62] T. Yajima.
"On the fundamental groups of knotted 2-manifolds in the 4-space".
In: *Journal of Mathematics, Osaka City University* 13.2 (1962),
pp. 63–71. URL: https://projecteuclid.org/journals/journal-of-mathematics-osaka-city-university/volume-13/issue-2/On-the-fundamental-groups-of-knotted-2-manifolds-in-the/ojm/1353055032.full.

[Yos94] K. Yoshikawa. "An enumeration of surfaces in four-space".
In: *Osaka Journal of Mathematics* 31.3 (1994), pp. 497–522.
URL: https://projecteuclid.org/journals/osaka-journal-of-mathematics/volume-31/issue-3/An-enumeration-of-surfaces-in-four-space/ojm/1200785461.full?tab=ArticleLink.

[Zee65] E. Zeeman. "Twisting spun knots". In: *Transactions of the American Mathematical Society* 115 (1965), pp. 471–195.
URL: https://www.ams.org/journals/tran/1965-115-00/S0002-9947-1965-0195085-8/S0002-9947-1965-0195085-8.pdf.